4. Experimental section

4.1. General methods and materials

All reactions were carried out under an atmosphere of argon. ^{1}H NMR spectra were obtained at 300 MHz on a Varian MERCURY 300 spectrometer with tetramethylsilane (TMS) as an internal standard in $CDCl_3$. ^{13}C NMR spectra were obtained at 75.45 MHz on a Varian MERCURY 300 spectrometer with $CDCl_3$ as an internal standard (δ 77.0) in $CDCl_3$. Mass spectra were recorded on Voyager System 4327 (Applied Biosystem). Analytical TLC was performed on Merck Kieselgel 60-F254 plates. Melting curves of nucleic acid duplexes were recorded on a UV-1650PC UV–visible spectrophotometer (Shimadzu). CD spectra were measured on a J-725 spectropolarimeter (JASCO). Fluorescence anisotropies were recorded on a FP-6500 spectrofluorometer (JASCO). Silica gel column chromatography was carried out using Silica gel 60 N (63–210 μm or 40–50 μm). Reversed phase HPLC was carried out using a μBondasphere 5-μm C4 or C18, 100 Å, 4 mm × 150 mm (Waters) with a gradient of 0–100% acetonitrile in water at 25 °C at a rate of 0.5 mL/min and acetonitrile and water is buffered by TFA (trifluoroacetic acid) with 0.05% v/v. Organic solvents were purified and dried by the appropriate procedure. RNA oligomers were purchased from Hokkaido System Science Co., Ltd and Japan Bio Services Co., Ltd. The yields of compounds were calculated from their dry weights except for **14**, **18** and **21**. The yields of **14** and **18** were estimated from absorbance compared with that of corresponding vitamin E derivatives. The yield of **21** was estimated from absorbance of $MMTr^+$ generated by deprotection.

4.1.1. Conditions for the UV melting analyses

Absorbance versus temperature profile measurements were carried out with eight-sample cell changer, in quarts cells of 1 cm pathlength. The variation of the difference of UV absorbance at between 260 nm and 320 nm with temperature was monitored. The temperature was scanned between 0 °C and 95 °C, and the rate of temperature increase was 0.2 °C/min. Oligonucleotides were annealed after addition of amino sugars. The samples containing oligonucleotides and amino sugars were first rapidly heated to 95 °C, left for 20 min, and then allowed to cool slowly to room temperature. These samples were furthermore cooled to 0 °C and left for 1 h, and then the dissociation was recorded by heating to 95 °C at rate of 0.2 °C/min.

4.1.2. Conditions for the CD spectrometry

All of the CD spectra were recorded at 25 °C. The following instrument settings were used: resolution, 0.1 nm; sensitivity, 10 mdeg; response, 4 s; speed, 10 nm/min; accumulation, 6.

4.1.3. Conditions for the fluorescence anisotropy measurement

The all titrations were measured at 20 °C. The following instrument settings were used: Ex/Em = 490 nm/520 nm; response, 2 s; Band width (Ex), 5 nm; Band width (Em), 5 nm; PMT voltage, 450 V; No. of cycle, 4;

4.2. Phenyl 2,6-dideoxy-2,6-diphthalimimde-1-thio-β-D-galactopyranoside (2)

Compound **1** (6.74 g, 16.8 mmol), triphenylphosphine (8.81 g, 33.6 mmol, 2.0 equiv), and phthalimide (4.94 g, 33.6 mmol, 2.0 equiv) were dissolved in dry tetrahydrofurane (168 mL) and cooled to 0 °C. To this mixture, diisopropyl azodicarboxylate (6.5 mL, 33.6 mmol, 2.0 equiv) was added dropwise over 20 min. After 40 min, further diisopropyl azodicarboxylate (3.0 mL) was added. After 30 min, methanol (20 mL) was added to the mixture and the solvent was evaporated. The crude product was recrystallized from methanol (50 mL) and then from ethyl acetate-hexane (1:5, v/v, 180 mL), and **2** was obtained as a colorless solid (6.28 g, 11.8 mmol, 71%).

^{1}H NMR ($CDCl_3$) δ 7.91–7.69 (m, 8H, N*Phth*), 7.39–7.34 (m, 2H, S*Ph*), 7.20–7.10 (m, 3H, S*Ph*), 5.59 (d, J = 10.2, 1H, H-1), 4.48–4.32 (m, 2H, H-2, H-3), 4.19–4.12 (m, 1H), 4.00–3.83 (m, 3H, 4-H), 3.62 (d, J = 5.1, 1H, 4-OH), 2.68 (d, J = 10.8, 1H, 3-OH).

^{13}C NMR ($CDCl_3$) δ 168.7, 134.6, 134.1, 132.7, 132.0, 131.8, 131.7, 131.6, 128.8, 127.9, 123.8, 123.7, 123.3, 84.0, 75.1, 68.6, 67.8, 53.1, 37.3.

MALDI-TOF MS: m/z calcd for $C_{36}H_{30}N_2NaO_8S$ $[M+Na]^+$: 553.10 Found: 553.11.

4.3. Phenyl 2,6-dideoxy-2,6-diphthalimimde-3-*O*-*p*-methoxybenzyl-1-thio-β-D-galactopyranoside (3)

Compound **2** (6.28 g, 11.8 mmol) was coevaporated with dry toluene (10 mL × 4) and dissolved in dry toluene (200 mL). Dibutyltin oxide (3.25 g, 13.0 mmol, 1.1 equiv) was added to the solution and it was refluxed for 12.5 h. Tetrabutylammonium iodide (4.81 g, 13.0 mmol, 1.1 equiv) and *p*-methoxybenzyl chloride (1.55 mL, 13.0 mmol, 1.1 equiv) was added. After 5.5 h, the mixture was cooled to rt and concentrated to dryness. The crude product was purified by silica gel column chromatography (dichloromethane (1.5% methanol)). The purified product was dissolved in toluene–dichloromethane–ethyl acetate (8:1:1, v/v/v, 500 mL) and washed with water (200 mL × 3). The product was further purified by silica gel column chromatography (dichloromethane (1.5% methanol)) and **3** was obtained as a colorless foam (7.35 g, 11.0 mmol, 93%).

^{1}H NMR ($CDCl_3$) δ 7.88–7.63 (m, 8H, N*Phth*), 7.23–7.16 (m, 2H, Ar), 6.97–6.82 (m, 5H, Ar), 6.45 (d, J = 8.7, 2H, Ar), 5.36 (d, J = 8.7, 1H, H-1), 4.57–4.50 (m, 2H, ArCH_2-a, H-2), 4.43–4.36 (m, 1H, H-5), 4.27–4.21 (m, 2H, ArCH_2-b, H-3), 4.08 (s, 1H, 4-H), 4.01–3.97 (m, 1H, H-6a), 3.82–3.76 (m, 1H, H-6b), 3.65 (s, 3H, CH_3OPh), 2.74 (d, J = 0.9, 1H, 4-OH).

^{13}C NMR ($CDCl_3$) δ 168.1, 167.9, 167.3, 159.1, 134.0, 133.9, 133.8, 132.9, 131.9, 131.8, 131.6, 131.5, 129.6, 129.0, 128.3, 127.6, 123.4, 123.1, 113.6, 83.7, 75.0, 74.9, 71.0, 66.0, 54.9, 50.7, 38.9.

MALDI-TOF MS: m/z calcd for $C_{36}H_{30}N_2NaO_8S$ $[M+Na]^+$: 673.16 Found: 673.08.

4.4. Phenyl 4-*O*-chloroacetyl-2,6-dideoxy-2,6-diphthalimimde-3-*O*-*p*-methoxybenzyl-1-thio-β-D-galactopyranoside (4)

Compound **3** (7.35 g, 11.0 mmol) was dissolved in a mixed solvent of pyridine-dichloromethane (1:20, v/v, 126 mL) and cooled to 0 °C. To the solution was added chloroacetyl chloride (1.75 mL, 22.0 mmol, 2.0 equiv). After 25 min, the solution was diluted with toluene and the solvent was evaporated. The crude product was purified by silica gel column chromatography (chloroform (0.5% ethanol)) and **4** was obtained as a colorless foam (7.39 g, 10.2 mmol, 93%).

^{1}H NMR($CDCl_3$) δ 7.88–7.60 (m, 8H, N*Phth*), 7.29–7.26 (m, 2H, Ar), 7.07–6.94 (m, 3H, Ar), 6.83 (d, J = 7.2, 2H), 6.38 (d, J = 8.4, 2H), 5.54 (d, J = 2.7, 1H, 4-H), 5.46 (d, J = 10.5, 1H, H-1), 4.45–4.23 (m, 6H, ClAc, ArCH_2-a, H-2, H-3, H-5), 4.12–3.98 (m, 2H, ArCH_2-b, H-6a), 3.88–3.81 (m, 1H, H-6b), 3.64 (s, 3H, CH_3OPh).

^{13}C NMR ($CDCl_3$) δ 167.9, 167.6, 167.4, 167.2, 159.1, 134.2, 133.9, 133.8, 133.0, 131.7, 131.5, 131.4, 129.8, 128.9, 128.5, 127.9, 123.5, 123.4, 123.1, 113.5, 83.9, 73.4, 72.8, 70.9, 68.0, 54.9, 51.1, 41.1, 38.1.

MALDI-TOF MS: *m/z* calcd for $C_{38}H_{31}ClN_2NaO_9S$ $[M+Na]^+$: 749.13 Found: 749.12.

4.5. Compound 5

Compound **4** (0.1452 g, 200 μmol) was coevaporated with dry toluene (2 mL × 4). *N*-Iodosuccinimide (0.1127 g, 500 μmol, 2.5 equiv) and 3-bromo-1-propanol (36 μL, 400 μmol, 2.0 equiv) were added and the mixture was dissolved in dichloromethane (1.0 mL). The solution was cooled and then 0.2% trifluoromethanesulfonic acid in diethyl ether (1.0 mL) was added. After stirring for 20 min, a saturated aqueous solution of $NaHCO_3$ (1 mL) was added and the mixture was warmed to rt. The solution was diluted with chloroform (30 mL), washed with a saturated aqueous solution of $NaHCO_3$ (30 mL) and 10% $Na_2S_2O_3$aq (30 mL). The organic layer was dried over Na_2SO_4, filtered, and concentrated. After the crude product was cooled to 0 °C, 7.5 mM sodium methoxide solution in methanol (10 mL) and dichloromethane (5 mL) was added to the mixture. After 12.5 h, Dowex 50 W × 8 (2 g) was added, and stirred for 30 min and the Dowex resin was removed by filtration. The crude product was purified by silica gel column chromatography (ethyl acetate–toluene (1:4, v/v)) to afford the pure β-glycoside **5** as a colorless oil (0.1156 g, 170 μmol, 85%).

^{1}H NMR ($CDCl_3$) δ 7.91–7.65 (m, 8H, N*Phth*), 6.95 (d, *J* = 8.7, 2H, Ar), 6.46 (d, *J* = 8.4, 2H, Ar), 5.04 (d, *J* = 8.4, 1H, H-1), 4.54 (d, *J* = 12.6, 1H), 4.48–4.41 (m, 1H), 4.32–4.22 (m, 3H), 4.01–3.92 (m, 3H), 3.73–3.65 (m, 4H), 3.48–3.40 (m, 1H), 3.18–3.14 (m, 1H), 2.83 (s, 1H), 1.95–1.74 (m, 2H).

^{13}C NMR ($CDCl_3$) δ 168.2, 167.7, 159.0, 134.1, 133.8, 133.7, 131.8, 131.5, 129.4, 129.1, 123.4, 123.3, 122.9, 113.4, 98.4, 74.3, 71.5, 71.1, 66.5, 65.6, 54.9, 52.0, 38.5, 32.1, 30.2.

4.6. Compound 6

A mixture of **5** (50.4 mg, 71 μmol) and **4** (77.6 mg, 106 μmol, 1.5 equiv) was coevaporatated with dry toluene (2 mL × 4). *N*-Iodosuccinimide (59.9 mg, 265 μmol, 3.75 equiv) was added and the mixture was dissolved in dichloromethane (0.5 mL). The solution was cooled, and then 0.04% trifluoromethanesulfonic acid in diethyl ether (1.5 mL) was added to the solution. After 1.5 h, a saturated aqueous solution of $NaHCO_3$ (1 mL) was added and the mixture was warmed to rt. The solution was diluted with chloroform (30 mL), washed with a saturated aqueous solution of $NaHCO_3$ (30 mL) and 10% $Na_2S_2O_3$aq (30 mL). The organic layer was dried over Na_2SO_4, filtered, and concentrated. After the crude product was cooled to 0 °C, 7.5 mM sodium methoxide solution in methanol (10 mL) and dichloromethane (5 mL) was added to the mixture. After 13 h, Dowex 50 W × 8 (1 g) was added, stirred for 30 min and the Dowex resin was removed by filtration. The crude product was purified by silica gel column chromatography (ethyl acetate–toluene (7:13, v/v)) to afford the pure β-glycoside **6** as a colorless oil (68.7 mg, 56.3 μmol, 79%).

^{1}H NMR ($CDCl_3$) δ 8.10 (d, *J* = 7.8, 1H, Ar), 7.88–7.00 (m, 17H, Ar),.6.51–6.17 (m, 6H, Ar), 5.24 (d, *J* = 8.1, 1H, H-1), 4.74 (d, *J* = 8.4, H-1), 4.68–4.58 (m, 2H), 4.47–4.25 (m, 4H), 4.15–3.45 (m, 18H), 3.33–3.25 (m, 1H), 3.11–3.06 (m, 2H), 2.84 (d, *J* = 3.0, 1H), 1.87–1.67 (m, 2H).

^{13}C NMR ($CDCl_3$) δ 168.8, 168.1, 168.0, 167.8, 167.4, 166.1, 159.1, 158.6, 133.9, 133.8, 133.3, 133.2, 132.9, 132.7, 132.2, 131.8, 131.6, 131.4, 129.5, 129.3, 124.5, 123.5, 123.3, 123.2, 122.7, 122.5, 122.0, 113.6, 113.4, 113.1, 99.8, 97.7, 75.1, 74.4, 73.8, 72.1, 71.6, 71.0, 66.2, 65.4, 55.0, 54.8, 52.0, 51.4, 40.1, 39.4, 32.3, 30.6.

MALDI-TOF MS: *m/z* calcd for $C_{93}H_{79}BrN_6NaO_{25}$ $[M+Na]^+$: 1241.26 Found: 1241.26.

4.7. Compound 7

The same procedure for the synthesis of **6** was applied to that of **7**, except for using **6** (0.0942 g, 77 μmol) and **4** (0.1056 g, 146 μmol, 1.9 equiv) as starting materials, and ethyl acetate–toluene (9:11, v/v) as eluting solvent in silica gel column chromatography. Compound **7** was obtained as a colorless oil (0.1044 mg, 59 μmol, 77%).

^{1}H NMR ($CDCl_3$) δ 8.35 (d, *J* = 7.2, 1H, Ar), 7.91–7.05 (m, 27H, Ar), 6.52–6.07 (m, 8H, Ar), 5.24 (d, *J* = 8.7, 1H, H-1), 4.94 (d, *J* = 7.8, 1H, H-1), 4.76–4.51 (m, 4H), 4.37–4.00 (m, 10H), 3.93–3.43 (m, 21H), 3.31–3.08 (m, 4H), 1.95–1.73 (m, 2H).

^{13}C NMR ($CDCl_3$) δ 169.2, 168.4, 168.1, 168.0, 167.9, 167.6, 167.3, 166.1, 165.8, 159.0, 158.5, 158.4, 133.9, 133.7, 133.6, 133.3, 133.1, 133.0, 132.8, 132.4, 132.2, 132.0, 131.8, 131.6, 131.3, 129.7, 129.6, 129.4, 129.1, 129.1, 125.2, 123.8, 123.3, 123.2, 123.1, 122.6, 122.3, 122.0, 121.7, 113.5, 113.0, 112.9, 99.6, 99.5, 97.5, 75.1, 74.3, 74.0, 73.8, 72.8, 71.7, 71.6, 71.0, 70.8, 70.6, 66.4, 65.3, 55.0, 54.8, 54.7, 52.1, 51.8, 51.3, 40.5, 40.4, 39.4, 32.4, 30.8.

MALDI-TOF MS: *m/z* calcd for $C_{93}H_{79}BrN_6NaO_{25}$ $[M+Na]^+$: 1781.42 Found: 1781.39.

4.8. Compound 8

Compound **7** (21.9 mg, 12.5 μmol) was dissolved in dichloromethane (5 mL) and cooled to 0 °C. To the solution, 20% trifluoroacetic acid in dichloromethane (5 mL) was added and stirred for 2 h. The reaction was quenched by addition of a saturated aqueous solution of $NaHCO_3$ (5 mL) and diluted with dichloromethane (60 mL). The solution was washed with a saturated aqueous solution of $NaHCO_3$ (100 mL) and the aqueous layer was back extracted with dichloromethane (20 mL × 3). The organic layer was dried over Na_2SO_4, filtered and concentrated. The crude product was purified by silica gel column chromatography (dichloromethane (3% methanol)) and **8** was obtained as a colorless oil (12.4 mg, 8.9 μmol, 71%).

^{1}H NMR ($CDCl_3$) δ 8.03–7.60 (24H, N*Phth*), 5.69 (d, *J* = 8.1, 1H, H-1), 5.46 (d, *J* = 7.8, 1H, H-1), 4.81 (d, *J* = 8.1, 1H, H-1), 4.62–4.56 (m, 1H), 4.34–3.59 (m, 18H), 3.51–3.44 (m, 1H), 3.25–3.17 (m, 2H), 3.04–2.93 (m, 4H), 1.95–1.73 (m, 2H).

^{13}C NMR ($CDCl_3$) δ 168.5, 168.2, 167.9, 134.4, 133.9, 133.7, 132.2, 131.9, 131.7, 131.6, 124.1, 123.8, 123.5, 123.1, 99.3, 99.1, 98.5, 75.4, 75.3, 72.6, 72.4, 72.3, 71.2, 69.6, 68.9, 68.5, 66.7, 54.4, 54.2, 53.6, 39.8, 37.6, 31.9, 30.3.

MALDI-TOF MS: *m/z* calcd for $C_{69}H_{55}BrN_6NaO_{22}$ $[M+Na]^+$: 1421.24 Found: 1420.91.

4.9. Compound 11

α-Tocopherol **10** (0.2495 g, 0.58 mmol) was dissolved in dry *N*,*N*-dimethylformamide (6 mL). To the solution, sodium hydride (60% purity, 91.6 mg, 2.3 mmol, 4 equiv) and propargyl bromide (200 μL, 2.3 mmol, 4 equiv) were added. After 2 h, methanol was added and the mixture was concentrated to dryness. The mixture was dissolved in dichloromethane (50 mL) and washed with water (30 mL × 2). The crude product was purified by silica gel column chromatography (dichloromethane-hexane (1:9, v/v)) to give **11** as a pale yellow oil (0.2229 g, 0.474 mmol, 82%).

^{1}H NMR ($CDCl_3$) δ 4.36 (d, *s* = 2.7, 2H, HC≡CCH_2O), 2.57 (t, *J* = 6.6, 2H, ArCH_2), 2.48 (d, *J* = 2.1, 1H, *H*C≡C), 2.20–2.08 (*s* × 3, 9H, ArCH_3), 1.81–0.83 (m, 38H).

^{13}C NMR ($CDCl_3$) δ 127.9, 126.0, 122.9, 117.5, 74.9, 74.5, 60.5, 40.0, 39.3, 37.4, 37.3, 32.8, 32.7, 31.2, 28.0, 24.8, 24.4, 23.9, 22.7, 22.6, 21.0, 20.6, 19.7, 19.6, 13.0, 12.2, 11.8.

4.10. Compound 13

Compound **8** (10.5 mg, 7.5 μmol) was coevaporated with dry toluene (1 mL × 3). Sodium azide (5.0 mg, 75 μmol, 10 equiv) was added and the mixture was dissolved in dry *N,N*-dimethylformamide (2 mL). The suspending solution was heated to 80 °C, stirred for 19 h and then cooled to rt. The solution was concentrated, diluted with ethyl acetate (20 mL), and washed with water (20 mL × 3). The aqueous layer was back extracted with toluene (20 mL) and the combined organic layer was dried over $MgSO_4$, filtered, and concentrated. To the crude product including **12**, **11** (14.2 mg, 30 μmol, 4 equiv) and copper powder (9.1 mg) were added. The mixed solvent (*t*-butanol–water (2:1, v/v, 3.0 mL)) was added to the mixture and the solution was stirred and heated to 65 °C. After 14 h, the solution was cooled to rt, filtered and purified by silica gel column chromatography (dichloromethane (3% to 4% methanol)) to afford the pure **13** as a colorless oil (9.0 mg, 4.9 μmol, 66%).

^{1}H NMR ($CDCl_3$) δ 8.02–7.60 (24H, N*Phth*), 7.49 (s, 1H, triazole-H), 5.69 (d, J = 8.7, 1H, H-1), 5.43 (d, J = 7.8, 1H, H-1), 4.83 (d, J = 7.8, 1H, H-1), 4.72 (s, 2H), 4.60 (m, 1H), 4.35–3.40 (m, 21H), 3.14–3.10 (m, 3H), 2.95 (d, J = 11.1, 1H), 2.58 (t, J = 6.6, 2H), 2.18–2.09 (s × 3, 9H), 1.88–0.80 (m, 40H).

^{13}C NMR (75.5 MHz, $CDCl_3$) δ 168.5, 168.2, 168.0, 148.0, 147.9, 144.4, 134.4, 133.9, 133.8, 132.1, 131.9, 131.7, 131.6, 131.5, 127.9, 126.0, 123.8, 123.5, 123.1, 122.9, 117.6, 99.5, 99.2, 98.5, 75.6, 74.8, 72.6, 72.2, 70.8, 69.6, 69.0, 68.5, 66.3, 65.6, 54.5, 54.1, 53.5, 47.0, 40.1, 39.8, 39.3, 37.5, 37.4, 37.3, 32.8, 32.7, 31.2, 30.2, 29.7, 28.0, 24.8, 24.4, 23.8, 22.7, 22.6, 21.0, 20.6, 19.7, 19.6, 12.9, 12.0, 11.8.

MALDI-TOF MS: *m/z* calcd for $C_{101}H_{107}N_9NaO_{24}$ $[M+Na]^+$: 1853.74 Found: 1852.79.

4.11. Compound 14

Compound **13** (3.9 mg, 2.1 μmol) was dissolved in ethanol (2.0 mL) and hydrazine monohydrate (60 μL) were added and the mixture was stirred and heated to 80 °C. After 4.5 h, the mixture was cooled to rt and concentrated. Eighth part of the entire crude product was purified by C4 reversed-phase HPLC (0.05% TFA, water-acetonitrile) and lyophilized from water to give **14** as a colorless solid (78.5 nmol, 29%).

MALDI-TOF MS: *m/z* calcd for $C_{53}H_{95}N_9NaO_{12}$ $[M+Na]^+$: 1072.70 Found: 1072.52.

4.12. Compound 16

Compound **15** (38.5 mg, 83 μmol) was coevaporated with dry toluene (10 mL × 4) and dissolved in dry tetrahydrofurane (1.5 mL). To the solution, sodium hydride (60% purity, 15.1 mg, 377 μmol, 4.5 equiv) and propargyl bromide (15 μL, 188 μmol, 2.3 equiv) were added. The mixture was heated to 60 °C and stirred for 16 h. After the solution was cooled to rt, methanol (1 mL) was added and concentrated. The crude product was dissolved in dichloromethane (30 mL) and washed with saturated brine (10 mL × 3) and the organic layer was dried over Na_2SO_4, filtered and concentrated. The crude product was dissolved in dry tetrahydrofurane (1.5 mL) and tetrabutylammonium fluoride (37.2 mg, 150 μmol) was added. After the solution was stirred for 20 min, the reaction was quenched by addition of saturated aqueous solution of $NaHCO_3$ and the solution was concentrated. The crude product was purified by silica gel column chromatography (dichloromethane-hexane (6:4, v/v)) to afford the pure **16** as a pale yellow oil (26.2 mg, 62 μmol, 75%).

^{1}H NMR ($CDCl_3$) δ 4.25 (s, 1H, Ar*OH*), 4.13 (d, J = 2.7, 2H, HC≡C*CH*$_2$O), 3.50 (t, J = 6.6, 2H, O*CH*$_2$CH$_2$), 2.59 (t, J = 6.9, Ar*CH*$_2$), 2.41 (t, J = 2.4, *HC*≡C), 2.15–2.10 (s × 2, 9H, Ar*CH3*), 1.81–1.22 (m, 21H).

^{13}C NMR (75.5 MHz, $CDCl_3$) δ 145.5, 144.5, 122.5, 121.0, 118.5, 117.3, 80.0, 74.4, 74.0, 70.3, 58.0, 39.4, 31.5, 30.1, 29.5, 29.5, 29.4, 26.0, 23.8, 23.6, 20.7, 12.2, 11.7, 11.3.

MALDI-TOF MS: *m/z* calcd for $C_{25}H_{39}O_3$ $[M+H]^+$: 387.3 Found: 386.8.

4.13. Compound 17

Compound **8** (4.5 mg, 3.2 μmol) was coevaporated with dry toluene (1 mL × 4), sodium azide (8.6 mg, 132 μmol, 41 equiv) was added and the mixture was dissolved in dry *N,N*-dimethylformamide (2.0 mL). The suspending solution was heated to 80 °C, stirred for 15 h and then cooled to rt. The solution was concentrated, dissolved in ethyl acetate (20 mL), and washed with water (20 mL × 3). The aqueous layer was back extracted with toluene (10 mL) and the combined organic layer was dried over $MgSO_4$, filtered, and concentrated. To the crude product including **12**, **16** (2.7 mg, 7.0 μmol, 2.2 equiv) and copper powder were added. Mixed solvent (*t*-butanol–water (2:1, v/v, 1.5 mL)) was added to the mixture and the solution was stirred and heated to 80 °C. After 3.5 h, the solution was cooled to rt, filtered and purified by silica gel column chromatography (dichloromethane (2.5–3.5% methanol)) to afford the pure **13** as a colorless oil (5.1 mg, 2.9 μmol, 91%).

^{1}H NMR ($CDCl_3$) δ 8.01–7.61 (24H, N*Phth*), 7.31 (s, 1H, triazole-H), 5.69 (d, J = 8.7, 1H, H-1), 5.44 (d, J = 8.4, 1H, H-1), 4.82 (d, J = 7.8, 1H, H-1), 4.63–4.56 (m, 1H), 4.50 (s, 2H), 4.40–3.37 (m, 26H), 3.13–3.07 (m, 3H), 2.91 (d, J = 11.1, 1H), 2.58 (t, J = 6.6, 2H), 2.14–2.10 (s × 3, 9H), 1.83–1.22 (m, 21H).

^{13}C NMR (75.5 MHz, $CDCl_3$) δ 168.6, 168.2, 168.0, 145.4, 144.8, 144.5, 134.5, 133.8, 132.1, 131.9, 131.5, 123.8, 123.5, 123.2, 122.5, 121.1, 118.6, 117.3, 99.4, 99.2, 98.4, 75.6, 74.5 72.6, 72.2, 70.7, 69.6, 69.0, 68.4, 65.4, 64.0, 54.5, 54.1, 53.5, 46.9, 39.9, 39.2, 37.5, 31.5, 30.1, 29.6, 29.5, 29.4, 26.1, 23.9, 23.5, 20.7, 12.3, 11.8, 11.3.

MALDI-TOF MS: *m/z* calcd for $C_{94}H_{93}N_9NaO_{25}$ $[M+Na]^+$: 1771.62 Found: 1770.43.

4.14. Compound 18

Compound **17** (5.1 mg, 2.9 μmol) was dissolved in ethanol (2.0 mL) and hydrazine monohydrate (60 μL) were added and the mixture was stirred and heated to 90 °C. After 4 h, the mixture was cooled to rt and concentrated. Four-twenty ninth of the entire crude product was purified by C18 reversed-phase HPLC (0.05% TFA, water–acetonitrile) and lyophilized from water to give **18** as colorless solid (235 nmol, 59%).

MALDI-TOF MS: *m/z* calcd for $C_{46}H_{81}N_9NaO_{13}$ $[M+Na]^+$: 990.59 Found: 990.49.

4.15. Compound 19

4-Monomethoxytrityl chloride (0.6416 g, 2.0 mmol) was dissolved in dry pyridine (20 mL) and stirred. To the solution, propargyl alcohol (150 μL, 2.54 mmol, 1.27 equiv) was added and stirred for 3 d. The solvent was evaporated. And the mixture was dissolved in dichloromethane (30 mL) and washed with saturated aqueous solution of $NaHCO_3$ (20 mL × 2). The aqueous layer was back extracted with dichloromethane (10 mL × 4). The combined organic layer was dried over Na_2SO_4, filtered and concentrated. The crude product was purified by silica gel column chromatography

(dichloromethane–hexane (3:1, v/v)) to afford the pure **19** as a colorless solid (0.5989 g, 1.82 mmol, 91%).

^{1}H NMR ($CDCl_3$) δ 7.49–7.45 (m, 4H, Ar), 7.37–7.20 (m, 8H, Ar), 6.87–6.82 (m, 2H, Ar), 3.80 (s, 3H, CH_3OAr), 3.75 (d, J = 2.4, HC≡CH_2), 2.39 (d, J = 2.4, HC≡CH_2).

^{13}C NMR ($CDCl_3$) δ 158.7, 143.8, 135.0, 130.2, 128.2, 127.9, 127.0, 113.2, 87.2, 80.5, 55.2, 52.7.

4.16. Compound 20

Compound **8** (4.2 mg, 3.0 μmol) was coevaporated with dry toluene (1 mL × 3), sodium azide (6.4 mg, 100 μmol, 33 equiv) was added and the mixture was dissolved in dry *N,N*-dimethylformamide (1.0 mL). The suspending solution was heated to 80 °C, stirred for 18 h and then cooled to rt. The solution was concentrated, dissolved in ethyl acetate (20 mL), and washed with water (20 mL × 3). The aqueous layer was back extracted with toluene (10 mL) and the combined organic layer was dried over $MgSO_4$, filtered, and concentrated. To the crude product including **12**, **19** (6.4 mg, 20 μmol, 6.7 equiv) and copper powder (3.8 mg) were added. Mixed solvent (*t*-butanol–water (2:1, v/v, 1.0 mL)) was added to the mixture and the solution was stirred and heated to 65 °C. After 12 h, the solution was cooled to rt, filtered and purified by silica gel column chromatography (dichloromethane (3% methanol)) to afford the pure **20** as a colorless oil (5.1 mg, 3.0 μmol, quant).

^{1}H NMR ($CDCl_3$) δ 8.04–7.23 (m, 37H, Ar), 6.84 (d, J = 9.0, 2H, Ar), 5.72 (d, J = 8.1, 1H, H-1), 5.49 (d, J = 8.1, 1H, H-1), 4.86 (d, J = 8.1, 1H, H-1), 4.62–4.55 (m, 1H), 4.35–3.42 (m, 26H), 3.21–3.03 (m, 3H), 2.80 (d, J = 11.7, 1H), 1.83–1.78 (m, 2H).

^{13}C NMR (75.5 MHz, $CDCl_3$) δ 168.6, 168.2, 167.9, 158.6, 145.5, 144.2, 135.4, 134.5, 134.0, 133.8, 132.1, 131.9, 131.7, 131.5, 130.3, 128.4, 127.9, 126.9, 124.1, 123.8, 123.6, 123.2, 122.3, 113.2, 99.3, 99.1, 98.5, 86.9, 78.5, 75.3, 72.7, 72.6, 72.3, 71.1, 69.7, 69.2, 68.3, 65.7, 58.6, 55.2, 54.5, 54.3, 53.6, 46.9, 39.8, 37.3, 30.1.

MALDI-TOF MS: m/z calcd for $C_{92}H_{75}N_9NaO_{24}$ $[M+Na]^+$: 1712.48 Found: 1712.16.

4.17. Compound 21

Compound **20** (5.1 mg, 3.0 μmol) was dissolved in dry ethanol (3.0 mL) and hydrazine monohydrate (90 μL) were added and the mixture was stirred and heated to 80 °C. After 4 h, the mixture was cooled to rt and concentrated. Eighth part of the entire crude product was purified by C18 reversed-phase HPLC (0.05% TFA, water–acetonitrile). A half of the purified product was dissolved in 80% aqueous solution of acetic acid (5 mL) and then the solvent was evaporated after 1.5 h. The product was dissolved to water (30 mL) and washed with dichloromethane (10 mL × 3). Water was evaporated and 1% aqueous solution of trifluoroacetic acid to the product. After coevaporation with water (2 mL × 3), the product was lyophilized from water to give **21** as a colorless solid (27 nmol, 14%).

MALDI-TOF MS: calcd for $C_{24}H_{47}N_9NaO_{11}$ m/z $[M+Na]^+$: 660.33 Found: 660.05.

4.18. Biological experiments

4.18.1. Cell culture

Rat hepatocellular carcinoma (McA-RH7777) cells were maintained in Dulbecco's modified Eagle's medium (Sigma–Aldrich, St Louis, MO) only or supplemented with 10% fetal bovine serum (Invitrogen, Carlsbad, CA), 100 units/ml penicillin, and 100 μg of streptomycin at 37 °C in 5% CO_2.

4.18.2. In vitro siRNA activity assay

To determine in vitro activity of siRNAs, McA-RH7777 cells (kindly gifted from Hiroyuki Arai, PhD) were transfected with 10 nM siRNAs in absence and presence of equally amount of compound **18** respectively using Lipofectamine™ 2000 (Invitrogen). The cells were harvested 24 h after transfection. Total RNA was extracted and the amount of endogenous *apoB* mRNA was measured by quantitative real-time polymerase chain reaction (qRT-PCR).

4.18.3. Quantitative RT-PCR assay

DNase-treated 2 μg of RNAs were reverse transcribed with Super Script III and Random Hexamers (Life Technologies, Carlsbad, CA). The cDNAs were amplified by the quantitative TaqMan system using the Light Cycler 480 Real-Time PCR Instrument (Roche Diagnostics, Mannheim, Germany). The primers and probes for rat *apoB* (NM_019287) and rat *glyceraldehyde-3-phosphate dehydrogenase* (*gapdh*; NM_017008) were designed by Applied Biosystems (Foster City, CA).

4.18.4. Statistical analysis

Student's two-tailed *t*-test was used to determine the significance of differences between control and transfected groups in quantitative RT-PCR assay. Data are presented as means ± standard error of the means (SEMs); P <0.05 was considered significant.

Acknowledgements

We thank the Japan Student Services Organization for the scholarship. And this work was supported by National Institute of Biomedical Innovation (NIBIO), KAKENHI (22·5612) and Japan Society for the Promotion of Science (JSPS).

Supplementary data

Supplementary data associated with this article can be found, in the online version, at http://dx.doi.org/10.1016/j.bmc.2013.12.060.

References and notes

1. Fire, A.; SiQun, X.; Mary, K. M.; Steven, A. K.; Samuel, E. D.; Craig, C. M. *Nature* **1998**, *391*, 806.
2. Davidson, B. L.; McCray, P. B. *Nat. Rev. Genet.* **2011**, *12*, 329.
3. Pecot, C. V.; Calin, G. A.; Coleman, R. L.; Lopez-Berestein, G.; Sood, A. K. *Nat. Rev. Cancer* **2011**, *11*, 59.
4. Kim, S.-S.; Garg, H.; Joshi, A.; Manjunath, N. *Trends Mol. Med.* **2009**, *15*, 491.
5. Castanotto, D.; Rossi, J. J. *Nature* **2009**, *457*, 426.
6. Rao, N. M. *Chem. Phys. Lipids* **2010**, *163*, 245.
7. Fröhlich, T.; Wagner, E. *Soft Matter* **2010**, *6*, 226.
8. Patil, M. L.; Zhang, M.; Betigeri, S.; Taratula, O.; He, H.; Minko, T. *Bioconjugate Chem.* **2008**, *19*, 1396.
9. Zhang, S.; Zhao, B.; Jiang, H.; Wang, B.; Ma, B. *J. Controlled Release* **2007**, *123*, 1.
10. Romøren, K.; Thu, B. J.; Bols, N. C.; Evensen, Ø. *Biochim. Biophys. Acta* **2004**, *1663*, 127.
11. Wightman, L.; Kircheis, R.; Rössler, V.; Carotta, S.; Ruzicka, R.; Kursa, M.; Wagner, E. *J. Gene Med.* **2001**, *3*, 362.
12. Iwata, R.; Sudo, M.; Nagafuji, K.; Wada, T. *J. Org. Chem.* **2011**, *76*, 5895.
13. Rigotti, A. *Mol. Aspects Med.* **2007**, *28*, 423.
14. Kappus, H.; Diplock, A. T. *Free Radical Biol. Med.* **1992**, *13*, 55.
15. Nishina, K.; Unno, T.; Uno, Y.; Kubodera, T.; Kanouchi, T.; Mizusawa, H.; Yokota, T. *Mol. Ther.* **2008**, *16*, 734.
16. Hosomi, A.; Arita, M.; Sato, Y.; Kiyose, C.; Ueda, T.; Igarashi, O.; Arai, H.; Inoue, K. *FEBS Lett.* **1997**, *409*, 105.
17. Nava, P.; Cecchini, M.; Chirico, S.; Gordon, H.; Morley, S.; Manor, D.; Atkinson, J. *Bioorg. Med. Chem.* **2006**, *14*, 3721.
18. Ito, H.; Ishida, H.; Kiso, M. *J. Carbohydr. Chem.* **2001**, *20*, 207.
19. Subramaniam, V.; Gurcha, S. S.; Besra, G. S.; Lowary, T. L. *Tetrahedron: Asymmetry* **2005**, *16*, 553.
20. Chang, R.; Moquist, P.; Finney, N. S. *Carbohydr. Res.* **2004**, *339*, 1531.
21. Brik, A.; Muldoon, J.; Lin, Y.-C.; Elder, J. H.; Goodsell, D. S.; Olson, A. J.; Fokin, V. V.; Sharpless, K. B.; Wong, C.-H. *ChemBioChem* **2003**, *4*, 1246.
22. Soutschek, J.; Akinc, A.; Bramlage, B.; Charisse, K.; Constien, R.; Donoghue, M., et al *Nature* **2004**, *432*, 173.

J Med Dent Sci 2013; 60: 9–16

Original Article

Efficient *in vivo* delivery of antisense oligonucleotide to choroid plexus

Wenying Piao[1)], Kazutaka Nishina[1,2)], Kie Yoshida-Tanaka[1)], Hiroya Kuwahara[1)], Tomoko Nishina[1)], Mina Sakata[1)], Hidehiro Mizusawa[1,2)] and Takanori Yokota[1,2)]

1) Department of Neurology and Neurological Science, Graduate School, Tokyo Medical and Dental University, Tokyo, Japan
2) JST-CREST

The choroid plexus (CP) is present on the ventricular walls of the brain, produces cerebrospinal fluid (CSF), contains many blood vessels, and is a major functional component of the blood-CSF barrier. The CP is an important site in the pathophysiology of various neurological diseases, including Alzheimer's disease and meningeal amyloidosis.
We performed gene silencing in the CP *in vivo* by using an antisense oligonucleotide (ASO). A short ASO of length 12 nucleotides was intravenously injected into rats. The ASO was not delivered to neurons or glia in the central nervous system, but was successfully delivered into the CP, and resulted in a significant reduction of endogenous target gene expression in epithelial cells within the CP. Although the mechanism of uptake of the ASO by the CP was not elucidated, the ASO bound to albumin *in vivo*, and the distribution of ASO delivery was similar to that of albumin delivery. These findings suggest that we inhibited target gene expression in the epithelial cells of the CP via albumin-ASO conjugates. This strategy should be useful for investigations of the function of CP, and for the development of new gene-silencing therapies for diseases with pathophysiology related to the CP.

Corresponding Author: Takanori Yokota, M.D., Ph.D.
Department of Neurology and Neurological Science Graduate School, Tokyo Medical and Dental University 1-5-45, Yushima, Bunkyo-ku, Tokyo 113-8519, Japan
Tel: +81-3-5803-5234 Fax: +81-3-5803-0169
E-mail: tak-yokota.nuro@tmd.ac.jp
Received September 27 ; Accepted November 16, 2012

Key words: antisense oligonucleotide, choroid plexus, drug delivery

Introduction

The choroid plexus (CP) is a highly vascularized tissue that is located in the brain ventricles and acts as the blood-cerebrospinal fluid barrier (BCSFB). The main function of the CP is secretion of cerebrospinal fluid (CSF), which is accomplished by active transport of small ions and water from the blood side to the CSF side. The CP also supplies the brain with certain nutrients, hormones, and metal ions, while removing metabolites from the CSF [1].

Antisense oligonucleotides (ASOs) have been in use for two decades, but recent advances have improved their effectiveness in gene silencing. Chemical modifications, particularly the use of locked nucleic acids (LNAs) [2, 3], markedly improve the binding affinity of ASOs to target RNA, resulting in more efficient steric-blocking. Furthermore, gapmer oligonucleotides, which contain two to five chemically modified nucleotides at both termini flanking a central 5 to 10-base 'gap' of DNA, enable cleavage of the target RNA by endogenous RNase H, which recognizes the DNA/RNA hybrid duplex [4]. The higher binding affinity of LNAs permits the development of far shorter ASOs, which was recently shown to increase gene silencing, probably due to increased intracellular availability [5].

The CP is associated with the pathophysiology of neurological diseases, such as Alzheimer's disease (AD) and meningeal amyloidosis. The delivery of ASO into the CP with an intracerebroventricular injection technique has been reported [6]; however, this technique cannot be applied clinically. Therefore, there is a need to develop an alternate strategy that is

clinically feasible.

Here, in order to demonstrate proof of concept for developing the delivery method of ASO to CP, we chose superoxide dismutase 1 (*Sod1*) as the target gene of endogenously expressed in CP, because its knock-out mice do not show any phenotype except for infertility [7], and so it is possible to evaluate the side effect of this delivery method.

In the present study, we have successfully delivered a phosphorothioate LNA-ASO (PS) targeting *Sod1* significantly inhibited the expression of *Sod1* mRNA in the CP of rats by intravenous injection demonstrating the feasibility of using this *in vivo* delivery system.

Materials and Methods

Design and synthesis of LNA-ASOs. An LNA-ASO that targeted rat *Sod1* was designed [8], and synthesized by Gene Design (Osaka, Japan). LNA-ASOs were synthesized with or without phosphorothioate (PS) linkages, and with or without Cy3-labeling as follows:
Rat *Sod1* LNA-ASO (PS), 5′-C*A*g*t*t*t*a*g*c*A*G*G -3′;
Cy3-labeled Rat *Sod1* LNA-ASO (PS), 5′-Cy3-C*A*g*t*t*t* a*g*c*A*G*G -3′; and
Cy3-labeled Rat *Sod1* LNA-ASO (PO), 5′-Cy3-CAgtttagcAGG-3′;
where the small letters represent DNA, the capital letters represent LNA, and the asterisks represent phosphorothioate linkages.

Histopathology. For pathological analysis of delivery of the LNA-ASO, 10 mg/kg Cy3-labeled LNA-ASO (PS) in phosphate-buffered saline (PBS) was injected into the tail vein of Female Crlj:CD1 (ICR) mice aged 4 wk or Sprague Dawley (SD) rats aged 3 wk (Oriental Yeast, Tokyo, Japan) at two time points (day 1 and day 4). Mouse albumin was fluorescent-labeled using Alexa Fluor Microscale Protein Labeling Kit (Life Technologies, Carlsbad, CA, USA), and 12 mg labeled albumin/kg body weight was injected into the tail vein of ICR mice aged 4 wk. The rodents were sacrificed by replacement of blood with PBS 24 h after the final injection. Brain tissue was fixed in 4% paraformaldehyde/PBS for 12 h. The fixed specimens were snap-frozen in liquid nitrogen and tissue sections with 10-μm thickness were prepared with the use of a LEICA CM3050 S cryostat (Leica Microsystems, Wetzlar, Germany). The sections were stained with Hoechst 33342 fluorescent stain (Sigma-Aldrich, St. Louis, MO, USA) to visualize the nuclei. The slides were analyzed by using a LSM 510 confocal laser scanning microscope (Carl Zeiss MicroImaging GmbH, Göttingen, Germany).

Fluorescence Correlation Spectroscopy (FCS) analysis. Fluorescence correlation spectroscopy measurements were obtained by using the ConfoCor 3 module in combination with an LSM 510 confocal microscope (Carl Zeiss MicroImaging) equipped with a C-Apochromat 40 ×/1.2 W objective. A HeNe laser (543 nm) was used to measure the excitation of Cy3-labeled LNA-ASOs in PBS, purified mouse albumin, the high density lipoprotein (HDL)-fraction of mouse serum, or mouse serum, the excitation of the mouse HDL-fraction of mouse serum labeled with Nile Red (Tokyo Chemical Industry, Tokyo, Japan), and the excitation of purified mouse albumin labeled by using the Alexa Fluor Microscale Protein Labeling Kit (Life Technologies). Emission was filtered through a 560-615 nm band pass filter. Samples were placed into an 8-well Lab-Tek chambered slide (Nalgene Nunc International, Rochester, NY, USA) and the diffusion time was measured at room temperature. Ten measurements with a sampling time of 20 s were obtained for each sample, and autocorrelation curves were fitted by using the ConfoCor 3 software package (Carl Zeiss MicroImaging) to determine the diffusion time.

Gel-shift assay. LNA-ASOs at a dose of 100 pmol were added to 0-640 μg of rat albumin. The samples were resolved by electrophoresis on a 15% polyacrylamide gel for 60 min at 100 V. The LNA-ASOs were visualized under ultraviolet light after treating the gel with ethidium bromide in Tris-borate-EDTA buffer.

Cell Culture. The Immortalized rat choroid plexus epithelial cell line (TR-CSFB) was kindly provided by Tetsuya Terasaki, PhD, Tohoku University. The TR-CSFB cells were maintained in DMEM (Sigma-Aldrich, St Louis, MO, USA) supplemented with 10% fetal bovine serum (Invitrogen, Carlsbad, CA, USA), 100 units/ml penicillin, and 100 µg of streptomycin at 33℃ in 5% CO_2 [9].

***In vitro* activity.** To determine the *in vitro* activity of the LNA-ASO (PS), Lipofectamine™ 2000 (Life Technologies) was used to transfect TR-CSFB cells with 10 nM or 50 nM of the LNA-ASO (PS) targeting rat *Sod1*. The cells were harvested 24 h after transfection. Total RNA was extracted and the amount of endogenous *Sod1* mRNA was measured by qRT-PCR.

***In vivo* activity.** Female wild-type Fischer 344 rats aged 10 wk (Oriental Yeast) were used for experiments measuring *in vivo* activity of the LNA-ASO (PS). The

rats were kept on a 12-h light/dark cycle in a pathogen-free animal facility with free access to food and water. Rat *Sod1* LNA-ASO (PS) was administered to the rats by tail-vein injection with the dosage based on body weight. PBS was used as the control, and administered by single injection. The CP was collected 3 d after the injection, and the level of *Sod1* mRNA was analyzed by quantitative real-time polymerase chain reaction (RT-PCR) assay.

All animal experiments were performed in accordance with the ethical and safety guidelines for animal experiments of the Tokyo Medical and Dental University (#0130113A).

Quantitative RT-PCR assay. Total RNA was extracted from cultured cells or rat brain CP homogenates with the use of Isogen (Nippon Gene, Tokyo, Japan). DNase-treated RNA (2 μg) was reverse-transcribed with Super Script Ⅲ and Random Hexamers (Life Technologies). The cDNAs were amplified by the quantitative TaqMan system by using the Light Cycler 480 Real-Time PCR Instrument (Roche Diagnostics, Mannheim, Germany). The primers and probes for rat *Sod1* and *Gapdh* were designed by Life Technologies. Relative *Sod1* mRNA levels were calculated in comparison to *Gapdh* mRNA levels.

Statistical analysis. All data represent means ± SEM (standard error of the mean). For FCS assays (Figure 3) and *in vitro* activity experiment (Figure 5), a one-way ANOVA followed by a Bonferroni-Dunn test used for multiple comparisons. For *in vivo* activity experiment (Figure 6), a Student's *t*-test was used to determine the significant differences between two groups.

Results

Delivery of LNA-ASO into CP via intravenous injection. After LNA-ASO targeting *Sod1* was injected into mice and rats intravenously, we histologically examined its distribution in brain tissue to assess the delivery efficiency. For this purpose, we utilized LNA-ASO that was 5′-end-labeled with Cy3. We injected each mouse with 10 mg/kg of LNA-ASO at days 1 and 4. The brains of the rodents were taken 24 h after the final injection, and frozen sections of the level of hippocampus, striatum and fourth ventricle were subjected to confocal laser imaging. We found robust Cy3 signals were observed in the CP of the nearby 3rd ventricle, lateral ventricle and 4th ventricle (Figure 1). These signals were distributed similarly to those in the CP of the mouse that was injected with Alexa Fluor-labeled mouse albumin (Figure 2).

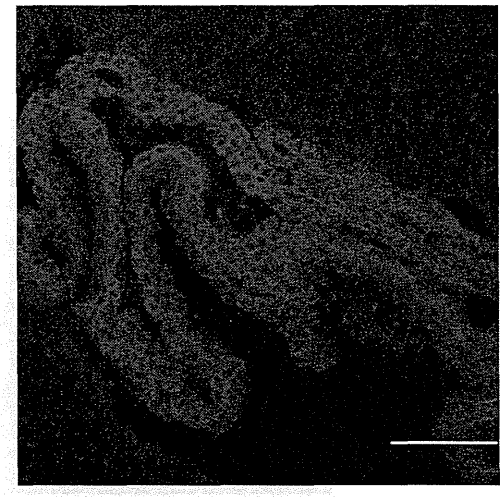

Figure 2. Intravenous injection-mediated delivery of albumin to the choroid plexus.
Confocal laser images of frozen mouse brain sections prepared after intravenous injection of Alexa Fluor 555-labeled purified mouse albumin. Red, Alexa Fluor 555-labeled mouse albumin; blue, Hoechst 33342. Scale bar = 100 μm.

***Ex vivo* binding of LNA-ASOs to albumin.** Because interactions between serum proteins and LNA-ASOs would influence pharmacokinetics, we next investigated the characteristics of serum proteins binding to LNA-ASO by performing an FCS analysis and gel-shift assay [10]. When LNA-ASO (PO), which does not have phosphorothioate-modified internucleotide linkages, was incubated with purified mouse albumin or the HDL fraction of mouse serum it migrated with almost the identical diffusion time as the same oligonucleotide incubated with PBS. In contrast, when LNA-ASO (PS), which has phosphorothioate modifications, was incubated with the mouse albumin it showed a much longer diffusion time than when it was incubated with PBS. In addition, it was not observed significant differences when it was bound to mouse serum (Figure 3). These results indicated that the interaction of the LNA-ASO (PS) with mouse albumin was due to the protein-binding property of the phosphorothioate-modifications of the LNA-ASO (PS). In the gel-shift assay, when the oligonucleotides were incubated without rat albumin, both LNA-ASO (PO) and LNA-ASO (PS) showed a band representing free LNA-ASO following separation of products on a 15% acrylamide gel. In contrast, LNA-ASO (PS) incubated with rat albumin did not show a band corresponding to free LNA-ASO (Figure 4).

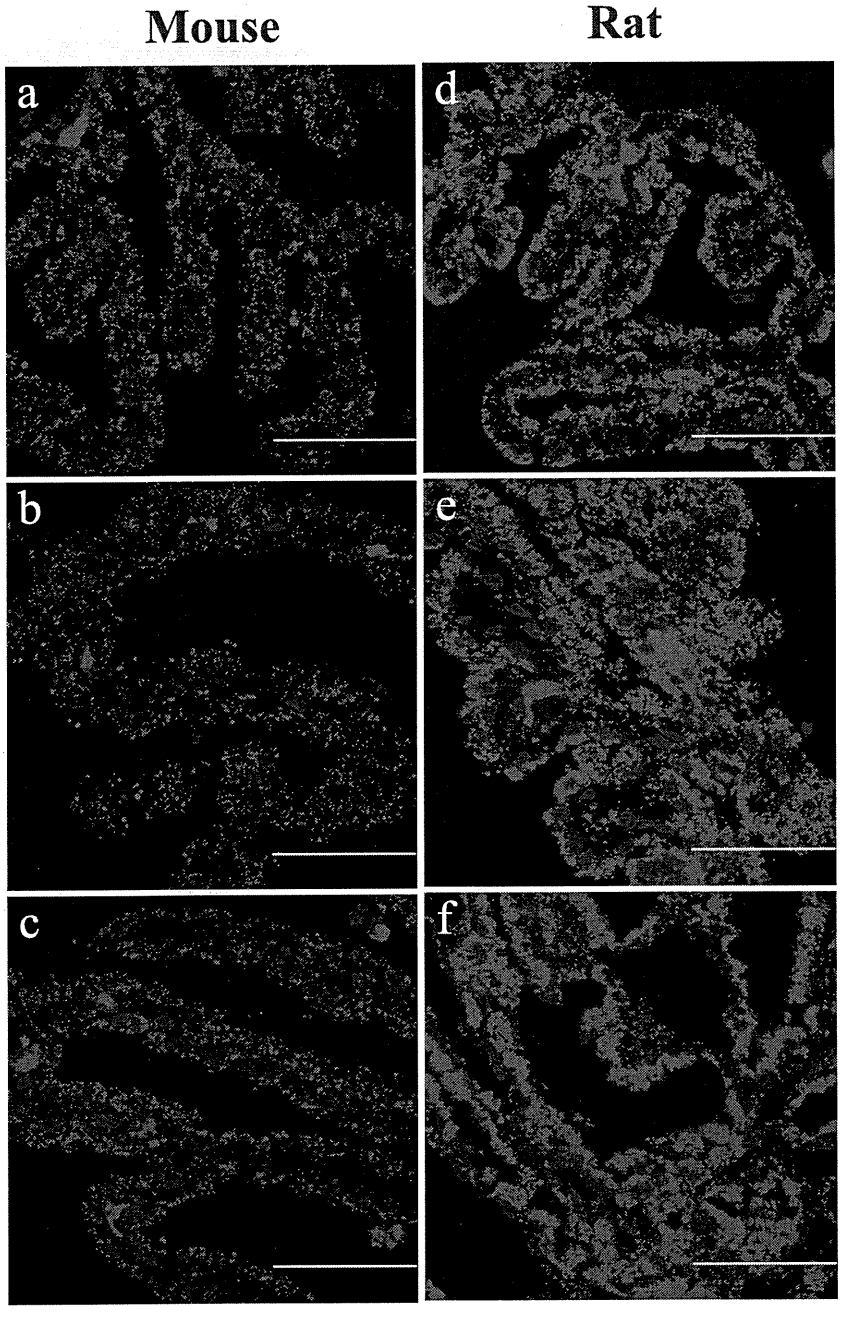

Figure 1. Intravenous injection-mediated delivery of LNA-ASO to mouse or rat choroid plexuses.
Confocal laser images of frozen mouse or rat brain sections prepared after intravenous injection of Cy3-labeled LNA-ASO (PS). Red, Cy3-labeled ASO; blue, Hoechst 33342. (a, b, c) and (d, e, f) shows mouse or rat choroid plexuses in the third ventricle, lateral ventricle, and fourth ventricle, respectively. Scale bar = 50 μm.

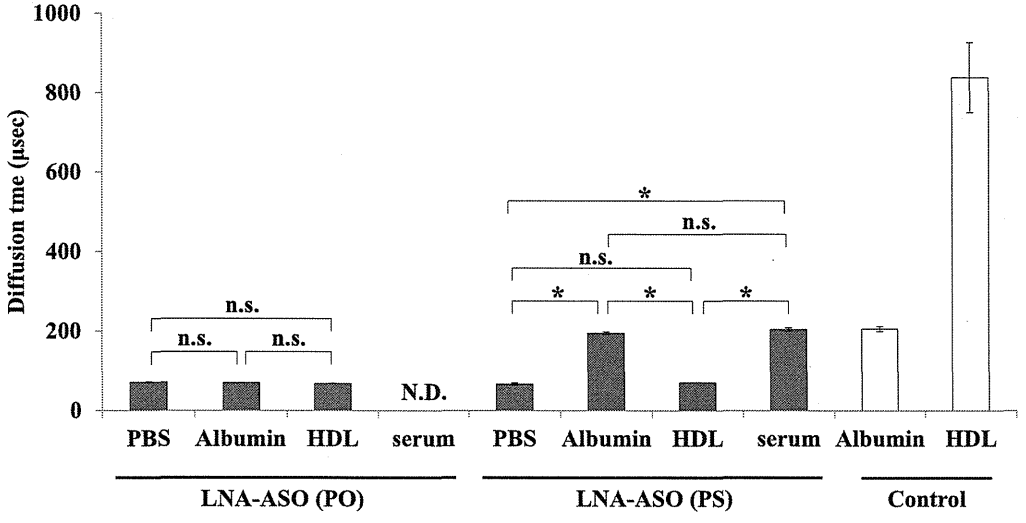

	LNA-ASO (PO)				LNA-ASO (PS)				Control	
	PBS	Albumin	HDL	serum	PBS	Albumin	HDL	serum	Albumin	HDL
Diffusion time (μsec)	71.6±1.0	70.4±0.7	68.4±0.5	N.D.	67.4±2.8	195.0±3.2	70.9±0.7	204.8±3.9	205.7±6.3	838.4±88.6

Values represent mean ± s.e.m. ($n = 10$). * $P < 0.01$.

Figure 3. *Ex vivo* assay of LNA-ASOs binding to mouse endogenous proteins.
Fluorescence correlation spectroscopy analysis of LNA-ASO with phosphodiester (LNA-ASO (PO)) or phosphorothioate (LNA-ASO (PS)) internucleotide linkages. A fixed volume (100 pmol) of each type of fluorescent-labeled LNA-ASO was incubated with PBS, purified mouse albumin, the HDL fraction of mouse serum, or mouse serum, and the diffusion time was measured. As a control, diffusion time of the fluorescent-labeled purified mouse albumin and the fluorescent-labeled HDL fraction of mouse serum were measured. The significant differences of the diffusion time, among PBS, Alubumin, HDL and serum, were tested using a one-way ANOVA followed by a Bonferroni-Dunn test, for LNA-ASO (PO) and LNA-ASO (PS) groups. N.D., Not Determined. n.s., not significant.

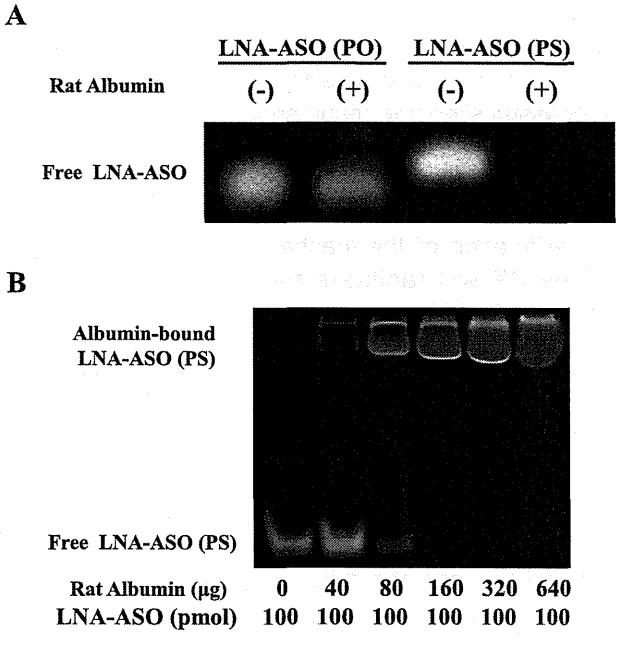

Figure 4. Gel-shift assay for the binding of LNA-ASOs to rat albumin.
(A) LNA-ASO (100 pmol) with phosphodiester (LNA-ASO (PO)) or phosphorothioate (LNA-ASO (PS)) internucleotide linkages was added to 0 or 160 μg of rat albumin and mixed. (B) LNA-ASO (PS) (100 pmol) was added to various amounts of rat albumin (0-640 μg) and mixed. The products were separated on a 15% acrylamide gel.

Effect of rat *Sod1* LNA-ASO (PS) on gene silencing *in vitro*. We examined the gene silencing effect of rat *Sod1* LNA-ASO (PS) *in vitro* by transfecting the oligonucleotide into cultured TR-CSFB cells. Rat *Sod1* LNA-ASO (PS) transfected at concentrations of 10 nM or 50 nM significantly inhibited the expression of the endogenous *Sod1* by 40% or 53%, respectively, relative to the level in the untreated cells (Figure 5). Thus, rat *Sod1* LNA-ASO (PS) was considered to be highly efficient and specific in its cleavage of *Sod1* mRNA.

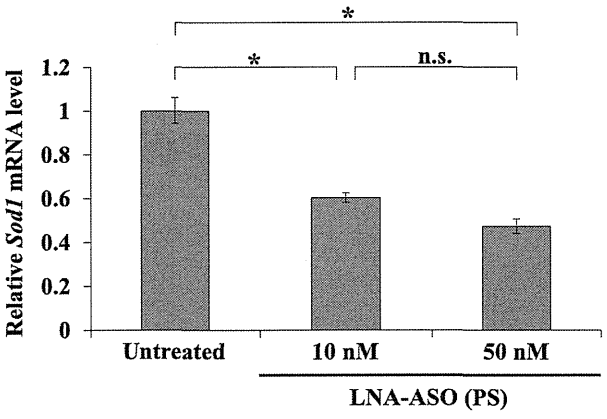

	Untreated	10 nM	50 nM
Sod1 mRNA level (% of untreated group)	100±6.1	60.4±2.2*	47.3±3.4*

Values represent mean ± s.e.m. ($n = 3$). * $P < 0.01$.

Figure 5. *In vitro* effect of the phosphorothioate LNA-ASO on gene silencing.
Reduction of rat *Sod1* mRNA levels in a rat choroid plexus epithelial cell line, TR-CSFB cells, after transfection with *Sod1* LNA-ASO (PS) (10 nM or 50 nM). Quantitative reverse-transcription polymerase chain reaction (qRT-PCR) analysis of rat *Sod1* mRNA levels relative to rat *Gapdh* mRNA levels was performed 24 h after transfection. Values are relative to those in untreated cells. One-way ANOVA followed by a Bonferroni-Dunn test were used for comparisons in the level of mRNA expression among 3 groups.

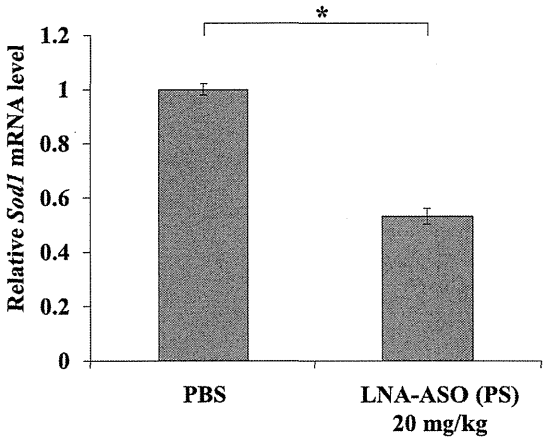

	PBS	LNA-ASO (PS) 20 mg/kg
Sod1 mRNA level (% of PBS group)	100±2.2	53.2±3*

Values represent mean ± s.e.m. ($n = 3$). * $P < 0.01$.

Figure 6. *In vivo* effect of the phosphorothioate LNA-ASO on gene silencing.
Quantitative reverse-transcription polymerase chain reaction (qRT-PCR) showing rat *Sod1* mRNA levels in rat choroid plexuses assayed 3 d after intravenous injection of rat *Sod1* LNA-ASO (PS) (20mg/kg). Values are relative to those in PBS only injected group. The data shown are relative to rat *Gapdh* mRNA levels. Student's *t*-test was used to determine the significant differences in mRNA expression level, between two groups (PBS vs LNA-ASO).

Gene silencing by intravenous injection of rat *Sod1* LNA-ASO (PS). We then assessed the extent of gene silencing after the intravenous injection of rat *Sod1* LNA-ASO (PS). Rats were injected with 20 mg/kg rat *Sod1* LNA-ASO (PS) and euthanized 3 d after the injection. To evaluate *Sod1* mRNA levels in CP, we conducted quantitative RT-PCR using total RNA extracted from CP homogenates. *Sod1* mRNA levels were significantly reduced by 47% in the treated animals when compared with the control animals (Figure 6).

Discussion

The results of this study demonstrated that intravenously administered 12 mer gapmer type phosphorothioate LNA-ASO targeting *Sod1* significantly inhibited the expression of *Sod1* mRNA in the CP of rats *in vivo*. When compared with untreated rats, the *Sod1* mRNA level was significantly decreased by about 50% in rats that were administered 20 mg/kg rat *Sod1* LNA-ASO (PS) to the tail vein. *In vitro* experiments similarly showed that the *Sod1* mRNA level was significantly decreased by up to 50% in a dose-dependent manner when rat *Sod1* LNA-ASO (PS) was transfected into a CP-derived cell line, TR-CSFB. There was one report in which endogenous gene of CP could not be suppressed by subcutaneously administered ASO [6], our successful silencing result should be due to the reports that a shorter gapmer type LNA-ASO is much more potent than a longer steric type 2'-O-(2-methoxy)-ethyl-modified ASO [5, 11].

Clarification of the mechanism of LNA-ASO delivery to the CP will facilitate the delivery of more LNA-ASO to the CP. In particular, the plasma protein-binding characteristics of LNA-ASOs will contribute to the understanding of the overall pharmacokinetic behavior of this class of ASOs. Watanabe et al. reported that phosphorothioate oligodeoxynucleotides bound mainly to albumin in the serum [10], and our results confirmed this finding. FCS analysis revealed that rat *Sod1* LNA-ASO (PS) bound to purified mouse albumin, not to HDL, and the diffusion time for rat *Sod1* LNA-ASO (PS) bound to purified mouse albumin was not significant different to that observed when it was bound to mouse serum (Figure 3). In addition, intravenously

injected purified mouse albumin was delivered to the CP with a similar distribution as that observed for intravenously injected LNA-ASO (Figures 1 and 2). We have reported previously that HDL-conjugated nucleic acids can be delivered to brain capillary endothelial cells (BCECs) [12]. Pardridge et al. reported a lack of albumin receptors in BCECs [13]. Therefore, our finding of active albumin uptake in the CP suggests that phosphorothioate LNA-ASOs could bind to endogenous serum albumin, and that the albumin could deliver the LNA-ASO to the CP.

The CP is associated with the pathophysiology of various neurological diseases, including AD and meningeal amyloidosis. *In vivo* silencing of key genes in the CP is a potentially useful approach for treating these diseases. In the case of AD, decreased amyloid β (Aβ) concentration in the CP might be associated with alterations in the activity of Aβ transporters [14]. With aging there is an increase in Aβ efflux transporter mRNA and lipoprotein receptor related protein (LRP)-1 and P-glycoprotein in CP epithelial cells, and a decrease in Aβ influx transporter mRNA and LRP-2 at the BCSFB. Potent inhibition of the Aβ influx transporter, LRP-2, would be expected to shift the equilibrium of Aβ between blood and CSF to the blood side, leading to reduction of Aβ in the brain.

Transthyretin (TTR), previously named prealbumin, is a homotetrameric protein. In the central nervous system, TTR is primarily synthesized and secreted into the CSF by the CP [15]. The expression and synthesis of TTR are independently regulated in blood and CSF [15]. TTR was the third CSF protein found to interact with Aβ, after apolipoprotein E [16] and clusterin [17]. It was hypothesized that these three extracellular proteins could "sequester" Aβ, thereby preventing neuronal damage [18]. Stein et al. reported that a lack of neurodegeneration was associated with increased levels of TTR in the hippocampus of a transgenic mouse model of AD, Tg2576 (APPsw) [19]. They also reported that chronic infusion of an antibody against TTR into the hippocampus of Tg2576 mice led to increased Aβ deposits, tau hyperphosphorylation, neuronal loss, and apoptosis in the cornu ammonis 1 (CA1) neuronal field [20]. In contrast, brain Aβ content and senile plaque in the brain was reduced when Tg2576 mice were crossed with $TTR^{-/-}$ mice, indicating that brain TTR accelerates the Aβ burden [21]. The role of CSF secreted from the CP in AD is controversial, but down-regulation of TTR in CP may improve AD pathology. Therefore, the epithelial cells in CP are a possible target site for gene therapies to treat AD.

Gene mutations in the TTR gene are commonly associated with a sensorimotor peripheral neuropathy called familial amyloidotic polyneuropathy, but a rare variant (D18G, G53E, A25T, L12P) is associated with oculoleptomeningeal amyloidosis or leptomeningeal amyloidosis, of which the main pathological features are TTR amyloid deposition within the leptomeningeal vessel walls and the pia-arachnoid membranes [22-25]. Clinical features may include dementia, ataxia, spasticity, seizures, radiculopathy, subarachnoid hemorrhage, and impaired consciousness. In this autosomal dominant disease, the mutant brain TTR derived from the CP is expected to cause detrimental conformational changes in the TTR tetramer and altered TTR deposition in the brain, leading to neurological symptoms. In this context, down-regulation of TTR in the CP in patients harboring TTR mutations is expected to cure or prevent the disease and symptoms.

The CP is a major functional structure of the BCSFB, which acts together with the blood-brain barrier (BBB) to protect the central nervous system from blood. The BCSFB prevent not only pathogens but also medical drugs from passing from the blood to the brain. Therefore, the difficulty in delivering drugs across the BCSFB and BBB is one of the major problems for treatment of brain diseases. We demonstrated that LNA-ASO injected via the tail vein could not pass through the BCSFB, but LNA-ASO reached the CP. Therefore another possible application of our method is the use of LNA-ASO to regulate BCSFB barrier function by regulating the key CP genes involved in this function.

In summary, this is the first report of CP-targeted ASO delivery using systemic administration. This method of ASO delivery can be advanced as a promising clinical strategy for gene silencing to treat various diseases involving the CP.

Acknowledgement

The authors thank Tetsuya Terasaki, Ph.D., Graduate School of Pharmaceutical Sciences, Tohoku University, and Kanjiro Miyata, Ph.D., Graduate School of Medicine, The University of Tokyo, for their helpful advices. This work was supported by grants from the Ministry of Health, Labour and Welfare of Japan (#2212070 and #2212148) and a grant from the Ministry of Education, Science and Culture of Japan (#20659138). The authors declare no conflict of interest.

References

1. Wolburg H, Paulus W. Choroid plexus: biology and pathology. Acta Neuropathol. 2010; 119(1): 75-88.
2. Obika S, Nanbu D, Hari Y, et al. Synthesis of 2′-*O*,4′-*C*-methyleneuridine and -cytidine. Novel bicyclic nucleosides having a fixed C_3, -*endo* sugar puckering. Tetrahedron Lett. 1997; 38(50): 8735-8.
3. Obika S, Nanbu D, Hari Y, et al. Stability and structural features of the duplexes containing nucleoside analogues with a fixed N-type conformation, 2′-*O*,4′-*C*-methyleneribonucleosides. Tetrahedron Lett. 1998; 39(30): 5401-4.
4. Wahlestedt C, Salmi P, Good L, et al. Potent and nontoxic antisense oligonucleotides containing locked nucleic acids. Proc Natl Acad Sci U S A. 2000; 97(10): 5633-8.
5. Straarup EM, Fisker N, Hedtjärn M, et al. Short locked nucleic acid antisense oligonucleotides potently reduce apolipoprotein B mRNA and serum cholesterol in mice and non-human primates. Nucleic Acids Res. 2010; 38(20): 7100-11.
6. Benson MD, Smith RA, Hung G, et al. Suppression of choroid plexus transthyretin levels by antisense oligonucleotide treatment. Amyloid. 2010; 17(2): 43-9.
7. Matzuk MM, Dionne L, Guo Q, et al. Ovarian function in superoxide dismutase 1 and 2 knockout mice. Endocrinology. 1998; 139(9): 4008-11.
8. Smith RA, Miller TM, Yamanaka K, et al. Antisense oligonucleotide therapy for neurodegenerative disease. J Clin Invest. 2006; 116(8): 2290-6.
9. Kitazawa T, Hosoya K, Watanabe M, et al. Characterization of the amino acid transport of new immortalized choroid plexus epithelial cell lines: a novel *in vitro* system for investigating transport functions at the blood-cerebrospinal fluid barrier. Pharm Res. 2001; 18(1): 16-22.
10. Watanabe TA, Geary RS, Levin AA. Plasma protein binding of an antisense oligonucleotide targeting human ICAM-1 (ISIS 2302). Oligonucleotides. 2006; 16(2): 169-80.
11. Yamamoto T, Harada-Shiba M, Nakatani M, et al. Cholesterol-lowering action of BNA-based antisense oligonucleotides targeting PCSK9 in atherogenic diet-induced hypercholesterolemic mice. Mol Ther Nucleic Acids. 2012; 1(5): e22
12. Kuwahara H, Nishina K, Yoshida K, et al. Efficient *in vivo* delivery of siRNA into brain capillary endothelial cells along with endogenous lipoprotein. Mol Ther. 2011; 19(12): 2213-21.
13. Pardridge WM, Eisenberg J, Cefalu WT. Absense of albumin receptor on brain capillaries *in vivo* or *in vitro*. Am J Physiol. 1985; 249(3 Pt 1): E264-7.
14. Pascale CL, Miller MC, Chiu C, et al. Amyloid-beta transporter expression at the blood-CSF barrier is age-dependent. Fluids Barriers CNS. 2011; 8: 21.
15. Aldred AR, Dickson PW, Marley PD, et al. Distribution of transferrin synthesis in brain and other tissues in the rat. J Biol Chem. 1987; 262(11): 5293-7.
16. Strittmatter WJ, Weisgraber KH, Huang DY, et al. Binding of human apolipoprotein E to synthetic amyloid beta peptide: isoformspecific effects and implications for late-onset Alzheimer disease. Proc Natl Acad Sci USA. 1993; 90(17): 8098-102.
17. Ghiso J, Matsubara E, Koudinov A, et al. The cerebrospinal-fluid soluble form of Alzheimer's amyloid beta is complexed to SP-40, 40 (apolipoprotein J), an inhibitor of the complement membrane-attack complex. Biochem J. 1993; 293(Pt 1): 27-30.
18. Schwarzman AL, Gregori L, Vitek MP, et al. Transthyretin sequesters amyloid beta protein and prevents amyloid formation. Proc Natl Acad Sci USA. 1994; 91(18): 8368-72.
19. Stein TD, Johnson JA. Lack of neurodegeneration in transgenic mice overexpressing mutant amyloid precursor protein is associated with increased levels of transthyretin and the activation of cell survival pathways. J Neurosci. 2002; 22(17): 7380-8.
20. Stein TD, Anders NJ, DeCarli C, et al. Neutralization of transthyretin reverses the neuroprotective effects of secreted amyloid precursor protein (APP) in APPSW mice resulting in tau phosphorylation and loss of hippocampal neurons: support for the amyloid hypothesis. J Neurosci. 2004; 24(35): 7707-17.
21. Wati H, Kawarabayashi T, Matsubara E, et al. Transthyretin accelerates vascular Abeta deposition in a mouse model of Alzheimer's disease. Brain Pathol. 2009;19(1): 48-57.
22. Vidal R, Garzuly F, Budka H, et al. Meningocerebrovascular amyloidosis associated with a novel transthyretin mis-sense mutation at codon 18 (TTR D18G). Am J Pathol. 1996; 148(2): 361-6.
23. Brett M, Persey MR, Reilly MM, et al. Transthyretin Leu12Pro is associated with systemic, neuropathic and leptomeningeal amyloidosis. Brain. 1999; 122 (Pt 2): 183-90.
24. Ellie E, Camou F, Vital A, et al. Recurrent subarachnoid hemorrhage associated with a new transthyretin variant (Gly53Glu). Neurology. 2001; 57(1): 135-7.
25. Garzuly F, Vidal R, Wisniewski T, et al. Familial meningocerebrovascular amyloidosis, Hungarian type, with mutant transthyretin (TTR Asp18Gly). Neurology. 1996; 47(6): 1562-7.

Biomaterials 35 (2014) 4548–4556

Contents lists available at ScienceDirect

Biomaterials

journal homepage: www.elsevier.com/locate/biomaterials

siRNA delivery from triblock copolymer micelles with spatially-ordered compartments of PEG shell, siRNA-loaded intermediate layer, and hydrophobic core

Hyun Jin Kim [a], Kanjiro Miyata [b], Takahiro Nomoto [c], Meng Zheng [b], Ahram Kim [c], Xueying Liu [b], Horacio Cabral [c], R. James Christie [b], Nobuhiro Nishiyama [d], Kazunori Kataoka [a,b,c,e,*]

[a] Department of Materials Engineering, Graduate School of Engineering, The University of Tokyo, 7-3-1 Hongo, Bunkyo-ku, Tokyo 113-8656, Japan
[b] Center for Disease Biology and Integrative Medicine, Graduate School of Medicine, The University of Tokyo, 7-3-1 Hongo, Bunkyo-ku, Tokyo 113-0033, Japan
[c] Department of Bioengineering, Graduate School of Engineering, The University of Tokyo, 7-3-1 Hongo, Bunkyo-ku, Tokyo 113-8656, Japan
[d] Polymer Chemistry Division, Chemical Resources Laboratory, Tokyo Institute of Technology, R1-11, 4259 Nagatsuta, Midori-ku, Yokohama 226-8503, Japan
[e] Center for NanoBio Integration, The University of Tokyo, 7-3-1 Hongo, Bunkyo-ku, Tokyo 113-8656, Japan

ARTICLE INFO

Article history:
Received 11 December 2013
Accepted 9 February 2014
Available online 6 March 2014

Keywords:
siRNA delivery
Polyion complex micelle
Triblock copolymer
Hydrophobic interaction

ABSTRACT

Hydrophobized block copolymers have widely been developed for construction of polymeric micelles for stable delivery of nucleic acids as well as anticancer drugs. Herein, we elaborated an A-B-C type of triblock copolymer featuring shell-forming A-segment, nucleic acid-loading B-segment, and stable core-forming C-segment, directed toward construction of a three-layered polymeric micelle as a small interfering RNA (siRNA) vehicle. The triblock copolymer was prepared with nonionic and hydrophilic poly(ethylene glycol) (PEG), cationic poly(L-lysine) (PLys), and poly{*N*-[*N*-(2-aminoethyl)-2-aminoethyl] aspartamide} [PAsp(DET)] bearing a hydrophobic dimethoxy nitrobenzyl ester (DN) moiety in the side chain [PEG-PLys-PAsp(DET-DN)]. The resulting triblock copolymers spontaneously formed sub-100 nm-sized polymeric micelles with a hydrophobic PAsp(DET-DN) core as well as PEG shell in an aqueous solution. This micelle was able to incorporate siRNA into the intermediate PLys layer, associated with slightly reduced size and a narrow size distribution. The triblock copolymer micelles (TCMs) stably encapsulated siRNA in serum-containing medium, whereas randomly hydrophobized triblock copolymer [PEG-PLys(DN)-PAsp(DET-DN)] control micelles (RCMs) gradually released siRNA with time and non-PEGylated diblock copolymer [PLys-PAsp(DET-DN)] control micelles (DCMs) immediately formed large aggregates. The TCMs thus induced appreciably stronger sequence-specific gene silencing in cultured cancer cells, compared to those control micelles. The siRNA delivery with TCMs was further examined in terms of cellular uptake and intracellular trafficking. The flow cytometric analysis revealed that the cellular uptake of TCMs was more efficient than that of RCMs, but less efficient than that of DCMs. The intracellular trafficking study using confocal laser scanning microscopy combined with fluorescence resonance energy transfer (FRET) revealed that the TCMs could readily release the siRNA payload within cells, which was in contrast to the DCMs exhibiting much slower release profile. This result indicates that PEG shell contributed to the smooth release of siRNA from TCMs within the cells, presumably due to avoiding irreversible aggregate formation. The obtained results demonstrated that the design of separately functionalized polymer segments expanded the performance of polymeric micelles for successful siRNA delivery.

1. Introduction

Small interfering RNA (siRNA), a trigger of RNA interference (RNAi), offers a new therapeutic modality for various intractable diseases, including cancer. To fulfill successful RNAi therapy, siRNA

* Corresponding author. Department of Materials Engineering, Graduate School of Engineering, The University of Tokyo, 7-3-1 Hongo, Bunkyo-ku, Tokyo 113-8656, Japan.
E-mail address: kataoka@bmw.t.u-tokyo.ac.jp (K. Kataoka).

http://dx.doi.org/10.1016/j.biomaterials.2014.02.016
0142-9612/

has generated the need for development of delivery vehicles, due to its biologically unstable nature and inefficient cellular uptake [1–3]. In this regard, block copolymers of neutral and hydrophilic poly(ethylene glycol) (PEG) and polycation have been developed as a promising delivery platform. The block copolymers electrostatically bind to oppositely charged siRNA to form a polyion complex (PIC) micelle having a distinctive core–shell structure, *i.e.*, PIC core for protecting siRNA payloads from enzymatic degradations and PEG shell for providing enhanced colloidal stability and reducing unfavorable interactions with biomacromolecules [4–6]. In particular, a sub-100 nm size of PIC micelles is preferable to deliver siRNA into solid tumors through the tumoral leaky vasculature, namely enhanced permeability and retention (EPR) effect [4,7–9]. Meanwhile, the electrostatic associations between siRNA and polycationic segment in the PIC core are inevitably interfered under biological conditions containing abundant charged biomacromolecules as a counterpart. Thus, to compensate such compromised stability of PIC micelles, additional stabilization approaches are required for successful siRNA delivery under harsh *in vivo* conditions.

So far, several stabilization approaches of PIC micelles have been explored by integrating stabilizing moieties, such as disulfide crosslinking [10–12], cholesterol groups [13–16], and long alkyl chains (*e.g.* stearoyl group) [17–21], into the polycationic segment. In particular, hydrophobic moieties can assist the spontaneous assembly of PICs through hydrophobic interactions in aqueous solutions, rendering PIC micelles more resistant to dissociation. Indeed, hydrophobic moieties have been randomly installed into polycationic segment in block copolymers without any specific arrangement [17–21]. Those hydrophobized block copolymers stabilized siRNA-loaded PIC micelles, demonstrating significant therapeutic effects in animal disease models bearing subcutaneous cancer or ischemia-reperfusion injury [20,21]. However, this "random modification" strategy may not fully utilize hydrophobic interactions, because hydrophilic siRNA and cationic moieties coexisting in the core probably interfere with the segregation of hydrophobic components in the core, leading to the compromised minimization of interfacial energy between shell and core [22–24]. Thus, we assumed that exclusion of hydrophilic siRNA payloads as well as polycationic segment from hydrophobic core allowed for more stable micelle formation. In this regard, our previous study installed a hydrophobic cholesterol moiety into ω-end of block copolymers, and the cholesterol-installed PIC micelles were significantly stabilized against the rapid dissociation in serum-containing medium [16]. Nevertheless, their moderate gene silencing efficiency *in vivo* suggested the necessity of further optimization of hydrophobic structures for improving the micelle performance.

An A-B-C type of triblock copolymer is a promising candidate for construction of polymeric micelles equipped with optimized hydrophobic core, because the C-segment can be elaborated with a variety of hydrophobic units. Thus, we herein synthesized a well-defined A-B-C triblock copolymer having hydrophilic PEG (A-segment), siRNA-loading cationic poly(L-lysine) (PLys) (B-segment), and hydrophobic core-forming polyaspartamide derivative (C-segment) (Fig. 1A). PLys having a high pK_a of ~10.5 was chosen to stably incorporate a negatively charged siRNA [25], as its binding affinity to nucleic acids is known to be relatively strong under biological conditions [26–28]. Also, polyaspartamide derivatives were prepared to regulate the hydrophobicity for enhanced micelle stability as well as uniform micelle formation, utilizing the aminolysis reaction with low molecular weight amine compounds [29]. The obtained triblock copolymers were characterized on their self-assembling behavior with or without siRNA in terms of size and its distribution. The triblock copolymer micelles (TCMs) were then examined on their stability in comparison with "randomly" hydrophobized control micelles (RCMs) (Fig. 1B) and non-PEGylated diblock copolymer control micelles (DCMs) (Fig. 1C). Cellular delivery of siRNA by those micelles was further compared in terms of the efficiencies of gene silencing, cellular uptake, and intracellular payload release, demonstrating the crucial roles of separately functionalized segments in TCMs for successful siRNA delivery.

2. Materials and methods

2.1. Materials

β-Benzyl-L-aspartate *N*-carboxy-anhydride (BLA-NCA) and ε-trifluoroacetyl-L-lysine *N*-carboxy anhydride [Lys(TFA)-NCA] were purchased from Chuo Kaseihin Co., Inc. (Tokyo, Japan). α-Methoxy-ω-amino-PEG (PEG-NH_2, M_n = 12,000) was obtained from NOF Co., Ltd. (Tokyo, Japan). *N,N*-Dimethylformamide (DMF), dichloromethane, diethylenetriamine (DET), methanol (MeOH), dimethylsulfoxide (DMSO), thiourea, diethylether, and *N*-methyl-2-pyrrolidone (NMP) were purchased from Wako Pure Chemical Industries, Ltd. (Osaka, Japan). Dulbecco's modified Eagle's medium (DMEM), diisopropylethylamine (DIPEA), and 4,5-dimethoxy-2-nitrobenzylchloroformate were purchased from Sigma–Aldrich Co. (St. Louis, MO). HEPES (1 M, pH 7.3) was purchased from Amresco (Solon, OH). DMF, DMSO, NMP, DET, and DIPEA were distilled with the conventional methods before use. Fetal bovine serum (FBS) and Alexa488-, Alexa546-, or Alexa647-labeled firefly luciferase siRNA (siLuc) were purchased from Invitrogen (Carlsbad, CA). Non-labeled siLuc (sense: 5′-CUU ACG CUG AGU ACU UCG AdTdT-3′; antisense: 5′-UCG AAG UAC UCA GCG UAA GdTdT-3′) and control siRNA (siCon) (sense: 5′-UUC UCC GAA CGU GUC ACG UdTdT-3′; antisense: 5′-ACG UGA CAC GUU CGG AGA AdTdT-3′) were synthesized by Hokkaido System Science Co., Ltd. (Hokkaido, Japan).

2.2. Synthesis of PEG-PLys(TFA)-PBLA

PEG-NH_2 (306 mg, 25.5 μmol) dissolved in DMF containing 1 M thiourea (DMF/thiourea, 4.5 mL) was added to Lys(TFA)-NCA solution (479 mg, 1.78 mmol) dissolved in DMF/thiourea (7.5 mL) [30]. The polymerization proceeded at 35 °C for 48 h under argon atmosphere. The resulting diblock copolymer was precipitated in diethylether three times and dried under reduced pressure overnight. The degree of polymerization (DP) of the Lys(TFA) unit was calculated to be 57 from ^{1}H NMR spectrum (10 mg/mL, 80 °C) based on the peak intensity ratio of the β, γ, and δ-methylene protons of lysine (–(CH_2)$_3$–, δ = 1.4–1.8) to the oxyethylene protons of PEG (–(OCH_2CH_2)–, δ = 3.7). For triblock copolymer, PEG-PLys(TFA) (300 mg, 12.2 μmol) in DMSO containing 1 M thiourea (DMSO/thiourea, 4.5 mL) was added to BLA-NCA solution (54.2 mg, 219 μmol) dissolved in DMSO/thiourea (1 mL). The polymerization proceeded at 35 °C for 48 h under argon atmosphere. The resulting triblock copolymer was precipitated in diethylether and dried under reduced pressure overnight. The DP of the BLA unit was calculated to be 18 from ^{1}H NMR spectrum (10 mg/mL, 80 °C) based on the peak intensity ratio between phenyl protons ($C_6H_5CH_2$–, δ = 7.3) in PBLA and ethylene protons (–(OCH_2CH_2)–, δ = 3.7) in PEG. The triblock copolymer was further characterized by gel permeation chromatography (GPC) (HLC-8220, TOSOH Corporation, Tokyo, Japan) equipped with two TSK gel columns (TSK-gel Super AW4000 and Super AW3000) through DMF containing LiCl (10 mM) at 0.8 mL/min. Molecular weight distribution (M_w/M_n) of the triblock copolymer was determined to be 1.08.

2.3. Synthesis of PEG-PLys(TFA)-PAsp(DET)

PEG-PLys(TFA)-PAsp(DET) (2) was prepared by the aminolysis reaction of PBLA with DET (Scheme S1) [18]. Briefly, PEG-PLys(TFA)-PBLA (1) (173 mg) was dissolved in NMP containing 1 M thiourea (NMP/thiourea, 8 mL) at 35 °C and cooled to 4 °C. Next, DET (0.6 mL) was diluted with NMP/thiourea (1.2 mL) and PEG-PLys(TFA)-PBLA solution was added dropwise into the DET solution. The mixture was stirred for 1 h at 15 °C under argon atmosphere. Then, the reaction mixture was added dropwise into ice-cold 5 M HCl (5 mL) for neutralization. The polymer product was purified by dialysis against 0.01 M HCl overnight and then deionized water for 2 h at 4 °C. The dialyzed solution was lyophilized to obtain the final product.

2.4. DN Introduction into DET moiety in PEG-PLys(TFA)-PAsp(DET)

First, a solution of PEG-PLys(TFA)-PAsp(DET) (2) (80 mg, 2.71 μmol) and distilled DIPEA (41 μL, 244 μmol) was prepared in MeOH/dichlorometane (4 mL, 1:1 v/v). Next, a solution of 4,5-dimethoxy-2-nitrobenzylchloroformate (26.9 mg, 0.0975 mmol) in dichloromethane (2 mL) was added dropwise to the PEG-PLys(TFA)-PAsp(DET) solution and the mixture was stirred for 24 h at 4 °C in the dark. The reaction was stopped by precipitation in diethylether (120 mL) and crude product was isolated by filtration. The filtered product was dissolved in MeOH/water (1:1 v/v) and dialyzed at 4 °C against 0.01 M HCl overnight and deionized water for 2 h in the dark. The final product was obtained by lyophilization.

2.5. Deprotection of TFA moiety in PEG-PLys(TFA)-PAsp(DET-DN)

PEG-PLys(TFA)-PAsp(DET-DN) (3) (60 mg) was dissolved in a mixed solvent of methanol (9 mL) and 1 N NaOH solution (1 mL) for 8 h at 35 °C. The mixture was

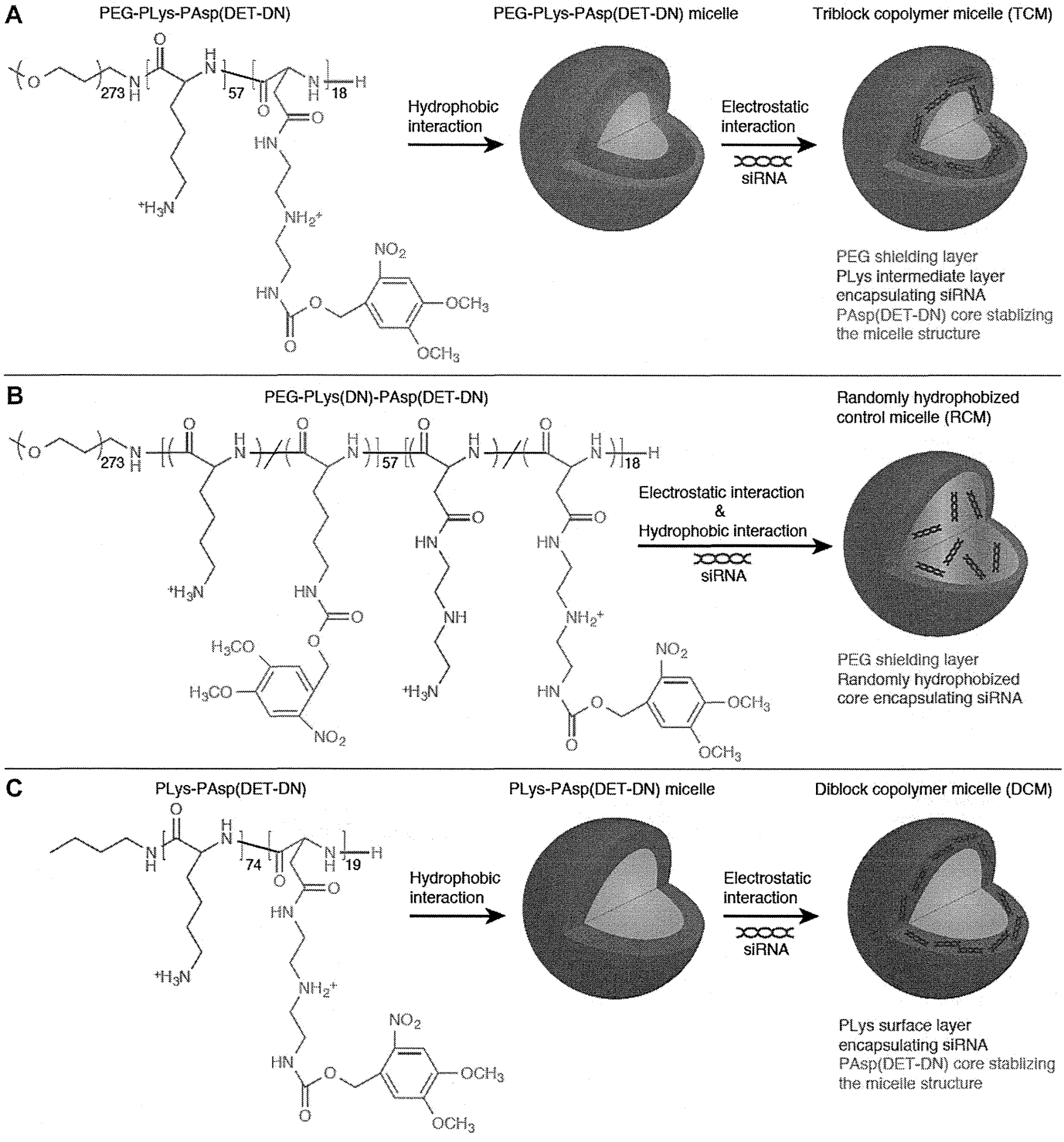

Fig. 1. Chemical structures of block copolymers developed in this study and schematic illustrations of hydrophobic triblock copolymer micelle (TCM; A), randomly hydrophobized control micelle (RCM; B), and diblock copolymer micelle without PEG shell (DCM; C).

dialyzed against 0.01 N HCl and then against deionized water. The final solution was lyophilized to obtain PEG-PLys-PAsp(DET-DN) (4) in the chloride salt form. The deprotection of the TFA groups was confirmed by ^{1}H NMR from the peak ratio of the methylene protons adjacent to the ε-amino group.

^{1}H NMR (D_2O/CD_3COOD): δ1.4–δ1.8 (342.9H, $COCH(CH_2)_3CH_2NH_3Cl$), δ2.7 (23.2H, $CHCH_2CONH$), δ3.0 (111.9H, $(CH_2)_3CH_2NH_3Cl$), δ3.3–δ3.4 (101.1H, $NH(CH_2)_2NH(CH_2)_2NH$), δ3.6 (1090H, OCH_2CH_2), δ3.8 (55.8H, $COCH_3COCH_3$), δ4.4 (56.5H, $COCHNH$), δ4.7 (14.0H, $COCHNH$), δ6.8 (26.0H, $CHCOCH_3COCH_3$), δ7.4 (24.1H, $COCH_3CHCNO_2$).

2.6. Micelle formation and siRNA loading

Polymeric micelles were prepared with PEG-PLys-PAsp(DET-DN) [or PLys-PAsp(DET-DN) as a non-PEGylated control] in an aqueous solution. The polymer (1 mg) was dissolved in 10 mM HEPES buffer (pH 7.3, 1 mg/mL) and incubated for 1 h in room temperature. Loading of siRNA in the polymeric micelles was performed by incubation of siRNA (20 μM in 10 mM HEPES buffer, pH 7.3) with the preformed polymeric micelles at the designated Amine/Phosphate ratios for 1–2 h in room temperature. The Amine/Phosphate ratio was defined as a residual molar ratio of

[primary amines in PEG-PLys-PAsp(DET-DN)]/[phosphates in siRNA]. Micelle size was determined at 25 °C using a Zetasizer (Malvern Instruments, Worcestershire, UK) equipped with a He–Ne Laser (λ = 633 nm) for the incident beam at a detection angle of 173°. Sample solutions were loaded into a low-volume quartz cuvette (ZEN2112, Malvern Instruments). The obtained data were analyzed by the cumulant method and the hydrodynamic (or cumulant) diameter of the micelles was then calculated by the Stokes–Einstein equation.

2.7. Transmission electron microscopy (TEM)

The shapes of micelles with or without siRNA were observed by a transmission electron microscope (JEM-1400, JEOL, Japan) operated with 100 kV acceleration voltages associated with 40 μA beam current. Micelle samples were placed on 400-mesh copper grids and stained using uranyl acetate solution (2% w/v).

2.8. Gel retardation assay

Gel electrophoresis was performed using 20% Novex polyacrylamide TBE gel (Invitrogen) under 100 V constant voltages for 60 min and then the gel was stained with SYBR Green II RNA Gel Stain (Invitrogen). Gels were imaged using Molecular Imager FX (Bio-Rad, Hercules, CA).

2.9. Fluorescence correlation spectroscopy (FCS)

FCS analyses were performed using a confocal laser scanning microscope, LSM510 (Carl Zeiss, Jena, Germany) equipped with a Confocor3 module and a Zeiss C-Apochromat 40 × water objective. A He–Ne laser (633 nm) was used for excitation of Alexa647-labeled siRNA and the emission was detected through above 650 nm. Samples were placed into an 8-well Lab-Tek chambered borosilicate cover-glass (Nalge Nunc International, Rochester, NY) and measured at room temperature. Stability of micelles containing Alexa647-labeled siRNA was evaluated in PBS containing 10% FBS (PBS/FBS). siRNA-loaded micelle solution (5 μM siRNA, Amine/Phosphate = 3) was diluted up to 100 nM siRNA with PBS/FBS, and then incubated at 37 °C for the designed period before measurements. Rhodamine 6G was used as a reference in 10 mM HEPES buffer (pH 7.3) to obtain a structural parameter in FCS analyses. Autocorrelation curves obtained from 10 measurements at a sampling time of 10 s were fitted with the Zeiss Confocor3 software package to calculate a diffusion coefficient of Alexa647-labeled siRNA.

2.10. In vitro luciferase gene silencing in cultured HeLa cells

Human cervical cancer cells stably expressing luciferase (HeLa-Luc) were seeded in 35 mm petri dishes (25,000 cells/dish) in DMEM containing 10% FBS (DMEM/FBS) and allowed to attach overnight. Then, the medium was removed and replaced with a fresh medium (2 mL) containing 100 μM luciferin and micelles (200 nM siRNA, Amine/Phosphate = 3). For each analysis, control samples were prepared by addition of medium diluted with 10 mM HEPES buffer (pH 7.3) instead of micelle solution. The added luciferin and micelle solution was 80 μL per 2 mL of medium. Samples were placed into a real-time photon-countable incubator (AB-2550 Kronos Dio, ATTO Corporation, Tokyo, Japan) and the luminescence intensity was measured periodically over 50 h at a temperature and CO_2 maintained at 37 °C and 5%, respectively. Relative luminescence intensity was determined by dividing the average luminescence intensity of treated samples by that of control samples ($n = 3$).

2.11. Cell viability assay

Cell viability was evaluated using a Cell Counting Kit-8 (Dojindo, Kumamoto, Japan). HeLa-Luc cells were seeded in a 96-well plate (5000 cells/well) in DMEM/FBS. After overnight incubation, siRNA-loaded micelles (Amine/Phosphate = 3) were added to the cells, and the cells were then incubated for 48 h. The micelle-containing medium was exchanged with a fresh medium (100 μL) containing the kit solution (10 μL), and the cells were further incubated for 1.5 h. The absorbance of the medium was measured at 450 nm using a microplate reader (Bio-Rad, Hercules, CA).

2.12. Flow cytometer measurement

HeLa-Luc cells were seeded in a 6-well plate (100,000 cells/well) in DMEM/FBS. Alexa647-labeled siRNA-loaded micelles were prepared with each polymer and added at 200 nM siRNA. After 4 h and 24 h incubation, the cells were washed twice with 0.5 mL of PBS, treated with a trypsin-EDTA solution, and suspended in PBS. The cellular uptake of siRNA-loaded micelles was measured using a flow cytometer (BD™ LSR II, BD Biosciences, San Jose, CA).

2.13. CLSM observation using FRET

HeLa-Luc cells (50,000 cells) were seeded in a 35-mm glass-based dish (Iwaki, Tokyo, Japan) and incubated overnight in DMEM/FBS. The micelles prepared with Alexa488-labeled siRNA and Alexa546-labeled siRNA (1:1 in molar ratio) at Amine/Phosphate = 3 were applied to the cells at 200 nM siRNA in fresh DMEM/FBS. Spectral images of the cells were obtained by LSM780 (Carl Zeiss, Oberkochen, Germany) equipped with a Plan-Apochromat 63 × objective (numerical aperture: 1.4) and the cells were incubated during CLSM observation in the incubator (Tokai Hit Co., Ltd., Shizuoka, Japan) at a temperature of 37 °C and a CO_2 concentration of 5%. The excitation wavelength was 488 nm (Ar laser) and the emission wavelength was 489–657 nm with the wavelength resolution of 8.8 nm. The spectral images were linearly unmixed into Alexa488 signal and Alexa546 signal, and FRET ratios in each pixel (Alexa546 signal/Alexa488 signal × 500) were calculated and expressed in a rainbow scale. All the image analyses were performed using ZEN software (Carl Zeiss).

Table 1
Hydrodynamic size, PDI, and ζ-potential of polymeric micelles without or with siRNA (Amine/Phosphate = 3).

Micelle	Polymer	Size (nm)/PDI/ζ-potential (mV) Without siRNA	Size (nm)/PDI/ζ-potential (mV) With siRNA
DCM	PLys-PAsp (DET-DN)	55/0.07/18.6	43/0.06/0.11
TCM	PEG-PLys-PAsp (DET-DN)	68/0.08/5.86	57/0.04/0.05
RCM	PEG-PLys(DN)-PAsp(DET-DN)	N.D.[a]	45/0.09/0.04

[a] The values were not determined due to substantially low scattered light intensity.

3. Results and discussion

3.1. Synthesis of block copolymers and their micelle characterizations

For construction of TCMs composed of hydrophilic shell, siRNA-loaded intermediate layer, and hydrophobic core, an A-B-C type of triblock copolymer was synthesized to have nonionic and hydrophilic PEG, cationic PLys, and hydrophobic polyaspartamide derivative (Fig. 1A). As a precursor, PEG-PLys(TFA)-PBLA was firstly synthesized by the sequential ring-opening polymerization of Lys(TFA)-NCA and then BLA-NCA, initiated by PEG-NH_2 as a macroinitiator (Scheme S1). The DP of PLys(TFA) and PBLA in the obtained triblock copolymer was determined to be 57 and 18, respectively, from ^{1}H NMR spectrum (Fig. S1). The DP of PLys(TFA) was designed to completely neutralize the negative charges of single siRNA (40 in 21mer/21mer) with single PLys chain. On the other hand, the DP of PBLA was targeted to be approximately 20, because our previous study revealed that the cationic polyaspartamide derivative modified with approximately 20 hydrophobic units significantly stabilized siRNA-loaded PICs in cell culture media [18]. The PBLA segment in PEG-PLys(TFA)-PBLA was aminolysed with DET, and then, the obtained PAsp(DET) segment was further modified with hydrophobic 4,5-dimethoxy-2-nitrobenzylchloroformate (DN) (Fig. 1A). The Asp(DET-DN) was developed here as a hydrophobic unit, because it enabled the micelle formation with a sub-100 nm size and a narrow size distribution, as demonstrated below. It should be noted that the utilization of ethylenediamine (–$NHCH_2CH_2NH$–) and triethylenetetramine [–$NH(CH_2CH_2NH)_3$–] linkers instead of DET [–$NH(CH_2CH_2NH)_2$–] resulted in larger micelle formation (>200 nm in diameter) associated with a larger size distribution [polydispersity index (PDI) in dynamic light scattering (DLS) > 0.1] (data not shown). These results suggest that fine-tuning of hydrophobic structures is crucial for the well-defined micelle formation. It should be further noted that the DN moiety is known to permit the carbamate cleavage via UV-irradiation, thus having the potential for external stimuli-responsive delivery [31,32]. Meanwhile, in order to verify the efficacy of hydrophobic C-segment on micelle stability, a control triblock copolymer, PEG-PLys(DN)-PAsp(DET-DN), was also synthesized by randomly introducing total 20 units of DN moieties into both PLys and PAsp(DET) segments (Fig. 1B). In addition, another control diblock copolymer, PLys-PAsp(DET-DN),

was synthesized from PLys(TFA)-PBLA for evaluating the effect of PEG on micelle properties (Fig. 1C).

Polymeric micelle formation with the obtained block copolymers was firstly evaluated in the absence of siRNA by DLS and ζ-potential measurements (Table 1) and TEM imaging (Fig. 2A). PEG-PLys-PAsp(DET-DN) successfully formed polymeric micelles having a cumulant diameter of 68 nm, a narrow size distribution (PDI = 0.08), and a moderately positive ζ-potential (~6 mV) in 10 mM HEPES buffer (pH 7.3). The narrow size distribution was also confirmed from the TEM image, which displays uniform and spherical structures having a number-averaged size of 20 ± 3 nm (n = 50). Considering that condensed nanostructures as well as phenyl derivatives can be effectively stained by uranyl acetate [33], these observed nanostructures are reasonably considered as a hydrophobic core composed of PAsp(DET-DN) segments. In a similar manner, PLys-PAsp(DET-DN) formed non-PEGylated diblock copolymer micelles that had a cumulant diameter of 55 nm, a PDI of 0.06, and a considerably positive ζ-potential (~19 mV) (Table 1). These results demonstrate that PAsp(DET-DN) segment with the DP of approximately 20 provided sufficient hydrophobicity to the block copolymers for micelle formation in aqueous solutions. It should be noted that the size and ζ-potential of PEG-PLys-PAsp(DET-DN) micelles were larger and lower, respectively, than those of PLys-PAsp(DET-DN) micelles, consistent with the presence of nonionic PEG shell in PEG-PLys-PAsp(DET-DN) micelles. On the other hand, the randomly hydrophobized triblock copolymer, PEG-PLys(DN)-PAsp(DET-DN), did not form such self-assemblies, as evidenced by a substantially lower scattered light intensity compared to PEG-PLys-PAsp(DET-DN) and PLys-PAsp(DET-DN) (Table S1). Taken together, it is indicated that a certain amount of sequential hydrophobic moieties in C-segment may be crucial for stable micelle formation with a hydrophobic core.

Next, siRNA was loaded into polymeric micelles by mixing siRNA solution with each micelle solution [or polymer solution for PEG-PLys(DN)-PAsp(DET-DN)]. The siRNA loading was confirmed by gel electrophoresis at various molar ratios of [primary amines in block copolymer]/[phosphates in siRNA] (Amine/Phosphate) ratios. Free siRNA band was not observed at Amine/Phosphate > 2 in TCMs and DCMs (Fig. S2), indicating complete encapsulation of siRNA within polymeric micelles. The cumulant size and ζ-potential of TCMs were decreased to 57 nm and 0.05 mV, respectively, and the narrow size distribution (PDI = 0.04) was maintained after polyionic complexation with siRNA at Amine/Phosphate = 3 (Table 1).

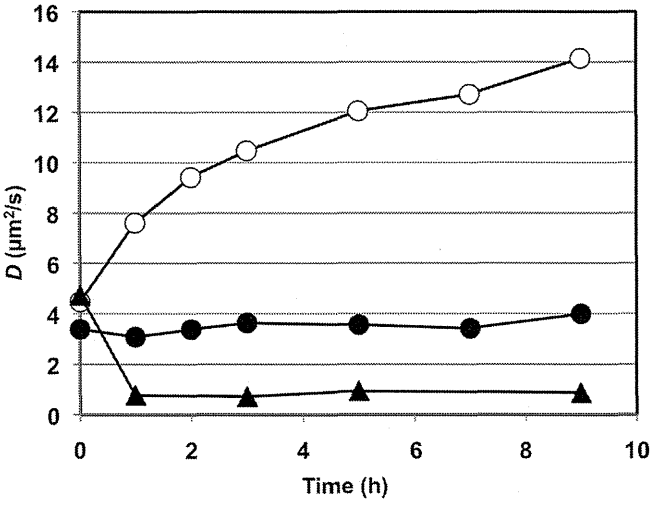

Fig. 3. Time-dependent changes in diffusion coefficient (D) of Alexa647-labeled siRNA loaded by DCMs (closed triangles), TCMs (closed circles), and RCMs (open circles) in PBS containing 10% FBS, measured by FCS.

Note that the similar cumulant size and size distribution were observed for the TCMs prepared at Amine/Phosphate ratios of 4 and 5 (Table S2), indicating that the well-defined micelle formation was not limited at a specific mixing ratio. The TEM image of siRNA-loaded TCMs depicts the formation of uniform and spherical nanostructures having a number-averaged size of 19 ± 2 nm (n = 50) (Fig. 2B). The similar complexation behavior was observed for the DCMs, which had the decreased cumulant size (43 nm) and ζ-potential (0.11 mV), associated with the low PDI of 0.06 (Table 1). These results indicate that negatively charged siRNAs were successfully bound to oppositely charged PLys segment within the preformed polymeric micelles without inducing secondary associations among the micelles. The almost similar sizes observed in the TEM images of TCMs with or without siRNA suggest that the hydrophobic PAsp(DET-DN) core should remain the same after the polyionic complexation. In contrast, the reduced cumulant sizes in the DLS analyses can be explained by shrinkage of the intermediate PLys layer in TCMs (or the outer layer in DCMs) through the polyionic complexation, presumably due to compromised electrostatic repulsion [34]. Altogether, the obtained results are consistent with our assumption that the TCMs should have the three-layered

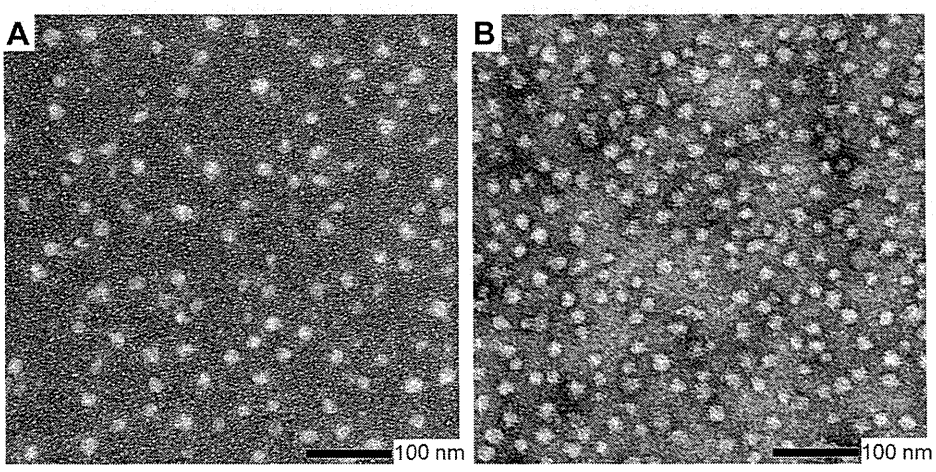

Fig. 2. TEM images of PEG-PLys-PAsp(DET-DN) micelles in the absence of siRNA (A) and in the presence of siRNA at Amine/Phosphate = 3 (B). Histograms of number-averaged size distribution of these TEM images were shown in Fig. S3. Scale bar represents 100 nm.

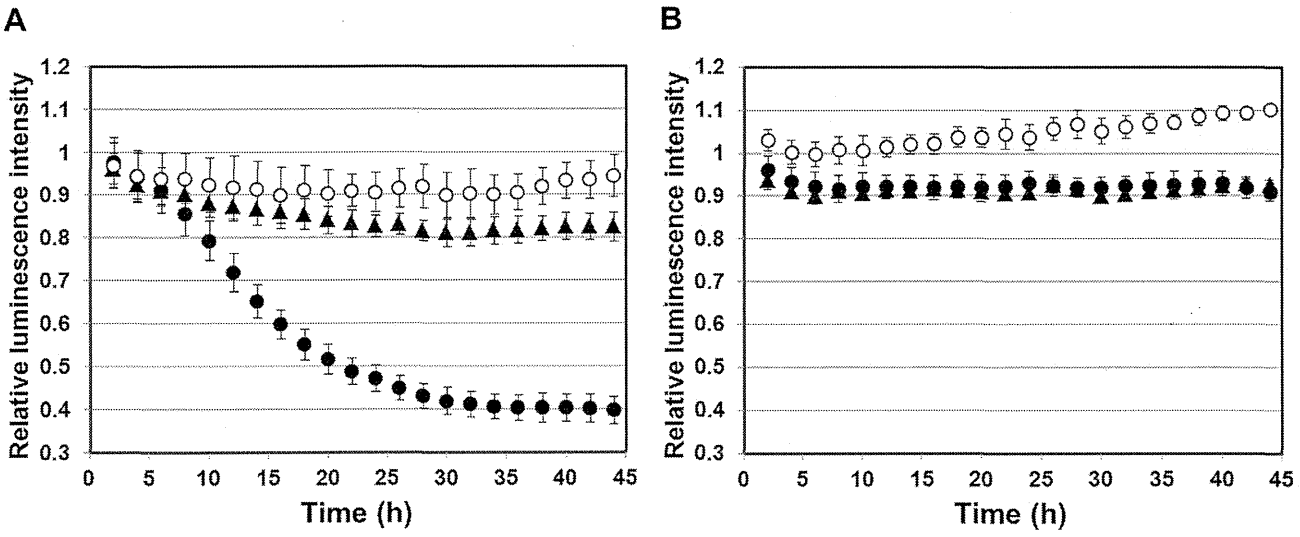

Fig. 4. Time dependent luciferase gene silencing of siRNA-loaded micelles, DCMs (closed triangles), TCMs (closed circles), and RCMs (open circles), in HeLa-Luc cells at 200 nM siRNA. A) siLuc and B) siCon. Results are expressed as the mean ± S.D. ($n = 3$).

structure featuring a hydrophobic core with the size of ~20 nm, siRNA/PLys PIC-based intermediate layer, and nonionic/hydrophilic PEG shell, as described in previous studies utilizing triblock copolymers composed of three different segments with varied electrostatic nature [35–38]. Meanwhile, PEG-PLys(DN)-PAsp(DET-DN) successfully formed PIC micelles (RCMs) with siRNA at Amine/Phosphate = 3 (Fig. S2), where their cumulant size, PDI, and ζ-potential were 45 nm, 0.09, and 0.04 mV, respectively (Table 1), through the charge-neutralization between the block copolymers and siRNAs. Based on the complete complexation of siRNA with a smaller amount of excess block copolymers, the micelle samples prepared at Amine/Phosphate = 3 were used in the following characterizations.

It was assumed that the micelle formation associated with the hydrophobic core should lead to higher stability in biological media containing charged biomacromolecules. Thus, the micelle stability in PBS/FBS was evaluated in terms of the change in diffusion coefficient (D), which was determined by FCS using fluorescently labeled siRNAs [16,18,19,28]. The micelle samples prepared with Alexa647-labeled siRNA at Amine/Phosphate = 3 were diluted with PBS/FBS, followed by the FCS measurement at different time points (Fig. 3). The initial D values of micelle samples (i.e. RCM, TCM, and DCM) were obviously lower than that of naked siRNA (56 ± 1 $\mu m^2/s$), consistent with the micelle formation between siRNAs and block copolymers. The D of RCMs gradually increased with time over 9 h, indicating micelle dissociation or siRNA release from the micelles. In contrast, the TCMs maintained their initial D over the incubation time, demonstrating the enhanced micelle stability in the culture medium due to the tightly packed hydrophobic core. The D of DCMs without PEG decreased immediately after dilution with PBS/FBS, indicating larger aggregate formation through adsorption of charged proteins onto the DCM surface. Altogether, it is concluded that both hydrophobic core and PEG shell should be essential for maintaining the siRNA-loaded micelle structure in the biological medium. The comparison of TCMs with previously reported, cholesterol-installed block copolymer micelles revealed the higher stability of TCMs, as indicated by the result that the D of the cholesterol-installed micelles reached that of naked siRNA after 1.5 h incubation in PBS/FBS [16]. The PAsp(DET) segment modified with sequentially-arranged 20 units of hydrophobic DN moieties would generate greater hydrophobicity compared to the single cholesterol moiety.

3.2. Cellular delivery of siRNA-loaded polymeric micelles

The gene silencing activity of siRNA-loaded micelles (Amine/Phosphate = 3) was investigated in cultured human cervical cancer cells stably expressing luciferase (HeLa-Luc). The luciferase-based luminescence intensity from the cells treated with each micelle was measured as an indicator of gene silencing by a photon-counting incubator (Fig. 4). Obviously, the TCMs showed the highest sequence-specific gene silencing efficiency among the tested micelles. In the cells treated with TCMs loading siLuc, the relative luminescence intensity progressively decreased with time and reached a plateau in approximately 30 h incubation. On the contrary, the TCMs loading siCon induced almost no decrease in relative luminescence intensity. Also, no significant cytotoxicity was observed in the cells treated with TCMs even at a high concentration of siRNA (2 μM) (Fig. S4), excluding the possibility of toxic effects on the decrease in luminescence intensity by TCMs with siLuc. On the other hand, DCMs and RCMs showed fairly weak gene silencing efficiency, compared to the TCMs (Fig. 4).

In order to elucidate the reason for the different gene silencing profiles among the tested micelles, a cellular uptake study was performed by a flow cytometer. Each micelle prepared with Alexa647-labeled siRNA (Amine/Phosphate = 3) was incubated with HeLa-Luc cells for 4 h and 24 h, and then the fluorescence intensity from the cells was measured (Fig. 5). All the micelle samples were more efficiently uptaken by the cells, compared to naked siRNA, presumably because of the adsorption and/or the partial exposure of polycationic segment contained in the micelles onto the oppositely charged cellular surface. In detail, RCMs and DCMs showed lower and higher cellular uptake efficiency, respectively, compared to TCMs at both time points. The lower cellular uptake of RCMs is probably due to their lower micelle stability in the serum-containing medium, as indicated in Fig. 3. The RCMs might gradually dissociate or release siRNA in the transfection medium, resulting in the compromised cellular entry of siRNA. This result is consistent with the appreciably lower gene silencing efficiency of RCMs, compared to TCMs. Meanwhile, the higher cellular uptake of DCMs might be explained by their non-PEGylated surface, which more likely facilitates the micelle adsorption onto the negatively charged cellular surface [39]. However, the efficient cellular uptake of DCMs is apparently inconsistent with their weak gene silencing efficiency in Fig. 4A. Thus, further studies are

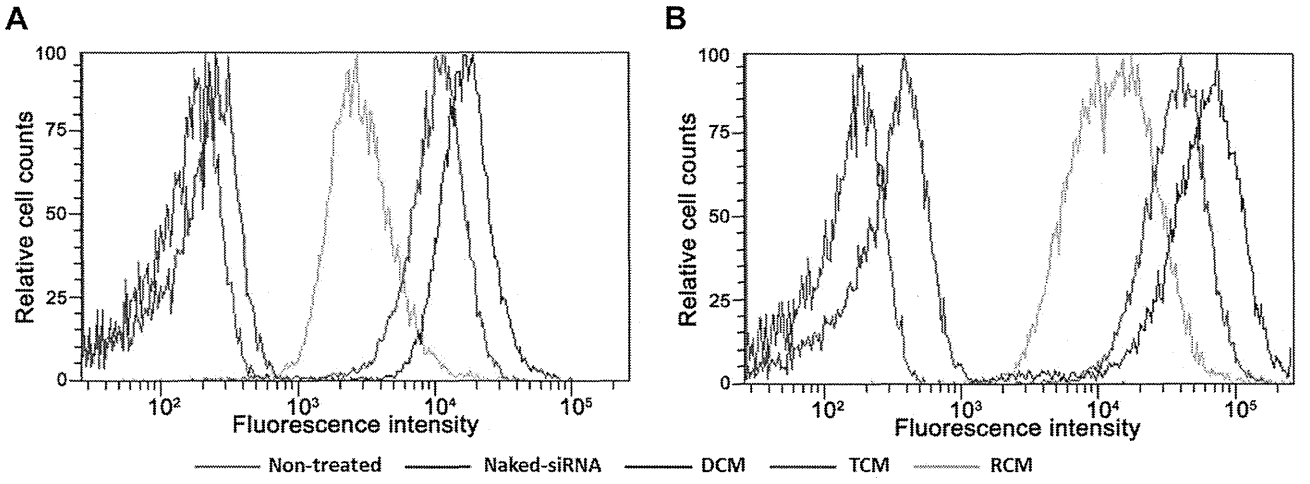

Fig. 5. Cellular uptake of Alexa647-labeled siRNA-loaded micelles (200 nM siRNA concentration, Amine/Phosphate = 3) in HeLa-Luc cells in 4 h (A) and 24 h (B) incubation.

required to explain about the different gene silencing efficiencies between TCMs and DCMs.

It is known that the transfer of siRNA from the endosome/lysosome to the cytoplasm is one of the critical steps for efficient gene silencing. Hence, the intracellular trafficking of fluorescently labeled siRNA-loaded micelles was examined by CLSM. Firstly, the colocalization of Alexa647-labeled siRNA with LysoTracker (Molecular Probes, Eugene, OR) that stains acidic cellular compartments (*i.e.* late endosome and lysosome) was observed after 24 h incubation as an indicator of endosomal escape efficiency (Fig. S5). Interestingly, there was no significant difference in the colocalization ratios of siRNA with late endosome/lysosome between TCMs and DCMs; Mander's coefficients of TCMs and DCMs were calculated to be 0.33 ± 0.12 and 0.50 ± 0.06 ($P > 0.05$), respectively, using Imaris software (Bitplane, Zurich, Switzerland).

We then assumed that siRNA release from the micelles within the cells might affect the gene silencing efficiency, because siRNA ultimately needs to be released and gain access to RNAi machinery in the cytoplasm. To investigate the release profile of siRNA, each micelle was prepared with both Alexa488-labeled siRNA and Alexa546-labeled siRNA (1:1 in molar ratio) to generate the FRET signal associated with the micelle formation [40]. Indeed, the excitation of Alexa488 allowed the adjacent Alexa546 within the micelle to emit the fluorescence via FRET, whereas the simple mixture of naked siRNAs did not show such a FRET signal (Fig. S6). The FRET pair-loaded TCMs or DCMs were incubated with HeLa-Luc cells and their FRET signal within the cells was observed by CLSM via the excitation at 488 nm. The FRET efficiency (Alexa546 intensity/Alexa488 intensity) in each pixel was calculated and expressed in a rainbow scale, where blue, green, and red indicate low, moderate,

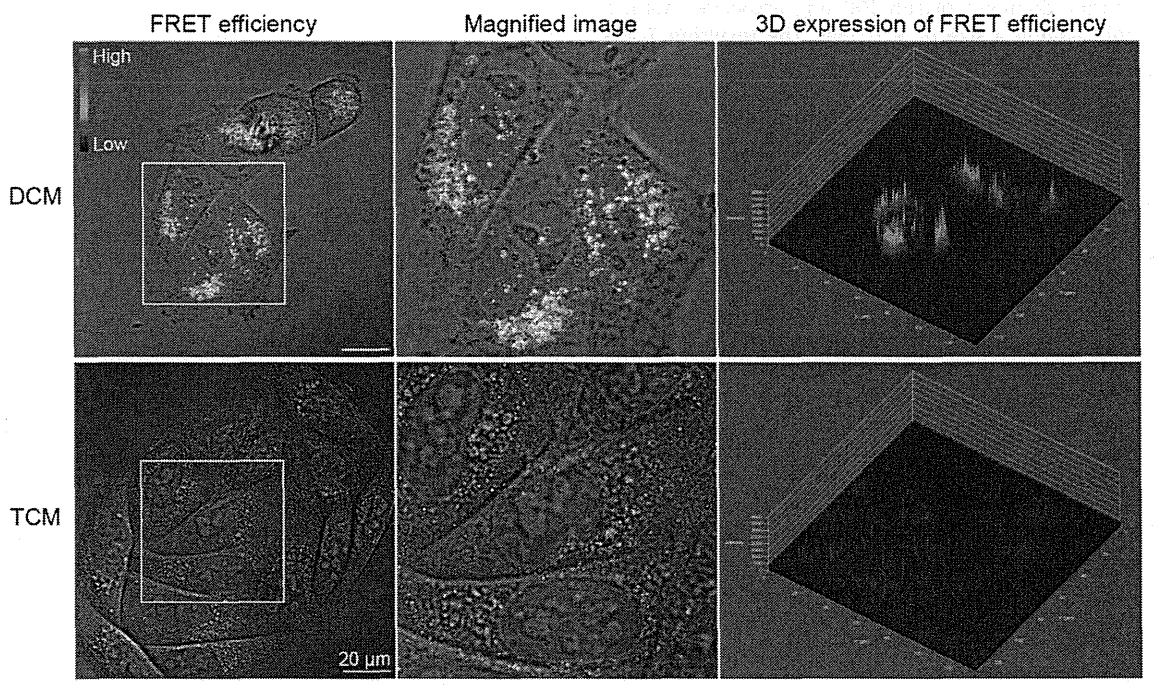

Fig. 6. FRET images of the micelles within cultured HeLa-Luc cells 12 h after the start of image acquisition. FRET ratio (Alexa546 intensity/Alexa488 intensity × 500) was calculated and expressed in a rainbow scale, where red, green, and blue signals mean high, moderate, and low FRET efficiency, respectively. The magnified images in the middle row correspond to the white squares in the left images. In the right row, the FRET efficiency was expressed in *z*-axis.

and high FRET efficiency, respectively (Fig. 6 and Movies S1–S2). The DCMs showed distinct red and green pixels, compared to TCMs, and maintained their higher FRET efficiency at least for 12 h. Considering that DCMs and TCMs showed similar FRET ratio in an aqueous solution as shown in Fig. S6, it is reasonable to conclude that DCMs did not effectively release siRNA in the cells, compared to TCMs. This ineffective release of siRNA might be explained by irreversible aggregate formation of DCMs in the serum-containing medium, as demonstrated in the FCS study (Fig. 3). In contrast, the cells treated with TCMs displayed more widely spreading and much lower FRET signals in the cell interior. Considering the result obtained from the intracellular trafficking study (Fig. S5), it is concluded that a major portion of the uptaken TCMs efficiently released siRNA payloads after endocytosis, whereas entrapped in late endosome/lysosome. It should be further noted that a minor portion of the released siRNAs should be located in the cytoplasm, as indicated by the significant gene silencing activity of TCMs (Fig. 4A). Note that a possible mechanism of the endosomal escape of TCMs is the endosomal membrane destabilization induced by direct interactions between the endosomal membrane and the hydrophobized polycationic chains released from TCMs [15,20]. The smooth release of siRNA from TCMs within the cells is presumably due to the result that PEG shell should avoid the aggregate formation inside the cells as well as in the serum-containing medium. Therefore, the higher gene silencing activity of TCMs might be explained by their balanced stability for enduring in the cell culture medium and then releasing siRNA within the cells.

Supplementary video related to this article can be found at http://dx.doi.org/10.1016/j.biomaterials.2014.02.016

4. Conclusion

In this study, an A-B-C type of triblock copolymer, PEG-PLys-PAsp(DET-DN), was synthesized for construction of three-layered polymeric micelles featuring hydrophobic core, siRNA-loaded intermediate layer, and PEG shell. The triblock copolymer self-assembled into uniform and spherical micellar architectures having a hydrodynamic diameter of sub-100 nm, associated with a hydrophobic core having a size of ~20 nm. The resulting TCMs stably encapsulated siRNA in the biological medium without dissociation and aggregation, presumably due to the PAsp(DET-DN) core and PEG shell. Consequently, the TCMs achieved efficient sequence-specific gene silencing in cultured HeLa-Luc cells without cytotoxicity. The comparative studies of TCMs with control micelles (RCMs and DCMs) revealed that their greater gene silencing activity should be due to both the efficient cellular uptake and the smooth release of siRNA inside the cells. These results demonstrate that the sophisticated arrangement of functional segments in triblock copolymer expands the performance of polymeric micelles for successful siRNA delivery. The present formulation of TCMs can be further developed toward the stimuli-responsive siRNA delivery based on the DN moiety.

Acknowledgment

This work was supported by the Funding Program for World-Leading Innovative R&D on Science and Technology (FIRST Program) from the Japan Society for the Promotion of Science (JSPS), Grant-in-Aid for Scientific Research from the Japanese Ministry of Education, Culture, Sports, Science and Technology.

Appendix A. Supplementary data

Supplementary data related to this article can be found at http://dx.doi.org/10.1016/j.biomaterials.2014.02.016.

References

[1] Aagaard L, Rossi JJ. RNAi therapeutics: principles, prospects and challenges. Adv Drug Deliv Rev 2007;59:75–86.
[2] Whitehead KA, Langer R, Anderson DG. Knocking down barriers: advances in siRNA delivery. Nat Rev Drug Discov 2009;8:129–38.
[3] Wagner E. Polymers for siRNA delivery: inspired by viruses to be targeted, dynamic, and precise. Acc Chem Res 2012;45:1005–13.
[4] Kataoka K, Harada A, Nagasaki Y. Block copolymer micelles for drug delivery: design, characterization and biological significance. Adv Drug Deliv Rev 2001;47:113–31.
[5] Kakizawa Y, Kataoka K. Block copolymer micelles for delivery of gene and related compounds. Adv Drug Deliv Rev 2002;54:203–22.
[6] Christie RJ, Nishiyama N, Kataoka K. Delivering the code: polyplex carriers for deoxyribonucleic acid and ribonucleic acid interference therapies. Endocrinology 2010;151:466–73.
[7] Matsumura Y, Maeda H. A new concept for macromolecular therapeutics in cancer chemotherapy: mechanism of tumoritropic accumulation of proteins and the antitumor agent smancs. Cancer Res 1986;46:6387–92.
[8] Maeda H. Macromolecular therapeutics in cancer treatment: the EPR effect and beyond. J Control Release 2012;164:138–44.
[9] Cabral H, Matsumoto Y, Mizuno K, Chen Q, Murakami M, Kimura M, et al. Accumulation of sub-100 nm polymeric micelles in poorly permeable tumours depends on size. Nat Nanotechnol 2011;6:815–23.
[10] Kakizawa Y, Harada A, Kataoka K. Environment-sensitive stabilization of core-shell structured polyion complex micelle by reversible cross-linking of the core through disulfide bond. J Am Chem Soc 1999;121:11247–8.
[11] Miyata K, Kakizawa Y, Nishiyama N, Harada A, Yamasaki Y, Koyama H, et al. Block catiomer polyplexes with regulated densities of charge and disulfide cross-linking directed to enhance gene expression. J Am Chem Soc 2004;126:2355–61.
[12] Christie RJ, Matsumoto Y, Miyata K, Nomoto T, Fukushima S, Osada K, et al. Targeted polymeric micelles for siRNA treatment of experimental cancer by intravenous injection. ACS Nano 2012;6:5174–89.
[13] Wang Y, Gao S, Ye WH, Yoon HS, Yang YY. Co-delivery of drugs and DNA from cationic core-shell nanoparticles self-assembled from a biodegradable copolymer. Nat Mater 2006;5:791–6.
[14] Kim WJ, Christensen LV, Jo S, Yockman JW, Jeong JH, Kim YH, et al. Cholesteryl oligoarginine delivering vascular endothelial growth factor siRNA effectively inhibits tumor growth in colon adenocarcinoma. Mol Ther 2006;14:343–50.
[15] Oba M, Miyata K, Osada K, Christie RJ, Sanjoh M, Li W, et al. Polyplex micelles prepared from ω-cholesteryl PEG-polycation block copolymers for systemic gene delivery. Biomaterials 2011;32:652–63.
[16] Kim HJ, Ishii T, Zheng M, Watanabe S, Toh K, Matsumoto Y, et al. Multifunctional polyion complex micelle featuring enhanced stability, targetability, and endosome escapability for systemic siRNA delivery to subcutaneous model of lung cancer. Drug Deliv Transl Res 2014;4:50–60.
[17] Alshamsan A, Haddadi A, Incani V, Samuel J, Lavasanifar A, Uludag H. Formulation and delivery of siRNA by oleic acid and stearic acid modified polyethylenimine. Mol Pharmacol 2009;6:121–33.
[18] Kim HJ, Ishii A, Miyata K, Lee Y, Wu S, Oba M, et al. Introduction of stearoyl moieties into a biocompatible cationic polyaspartamide derivative, PAsp(-DET), with endosomal escaping function for enhanced siRNA-mediated gene knockdown. J Control Release 2010;145:141–8.
[19] Oskuee RK, Philipp A, Dehshahri A, Wagner E, Ramezani M. The impact of carboxyalkylation of branched polyethylenimine on effectiveness in small interfering RNA delivery. J Gene Med 2010;12:729–38.
[20] Kim HJ, Oba M, Pittella F, Nomoto T, Cabral H, Matsumoto Y, et al. PEG-detachable cationic polyaspartamide derivatives bearing stearoyl moieties for systemic siRNA delivery toward subcutaneous BxPC3 pancreatic tumor. J Drug Target 2012;20:33–42.
[21] Kim D, Hong J, Moon H, Nam HY, Mok H, Jeong JH, et al. Anti-apoptotic cardioprotective effects of SHP-1 gene silencing against ischemia-reperfusion injury: use of deoxycholic acid-modified low molecular weight polyethyleneimine as a cardiac siRNA-carrier. J Control Release 2013;168:125–213.
[22] Mya KY, Lin EMJ, Gudipati CS, Gose HB, He C. Self-assembly of block copolymer micelles: synthesis via reversible addition-fragmentation chain transfer polymerization and aqueous solution properties. J Phys Chem B 2010;114:9128–34.
[23] Moughton AO, Hillmyer MA, Lodge TP. Multicompartment block polymer micelles. Macromolecules 2012;45:2–19.
[24] Bates FS, Hillmyer MA, Lodge TP, Bates CM, Delaney KT, Fredrickson GH. Multiblock polymers: panacea or pandora's box? Science 2012;336:434–40.
[25] Harada A, Cammas S, Kataoka K. Stabilized α-helix structure of poly(L-lysine)-block-poly(ethylene glycol) in aqueous medium through supramolecular assembly. Macromolecules 1996;29:6183–8.
[26] Miyata K, Fukushima S, Nishiyama N, Yamasaki Y, Kataoka K. PEG-based block catiomers possessing DNA anchoring and endosomal escaping functions to form polyplex micelles with improved stability and high transfection efficacy. J Control Release 2007;122:252–60.
[27] Shimizu H, Hori Y, Kaname S, Yamada K, Nishiyama N, Matsumoto S, et al. siRNA-based therapy ameliorates glomerulonephritis. J Am Soc Nephrol 2010;21:622–33.